Evaluation of kraft and hydrolysis lignin hydroconversion over unsupported NiMoS catalyst

Chemical Engineering Journal 453 (2023) 139829

Contents lists available at ScienceDirect

Chemical Engineering Journal

journal homepage: www.elsevier.com/locate/cej

Evaluation of kraft and hydrolysis lignin hydroconversion over unsupported NiMoS catalyst

Abdenour Achour [a,*], Diana Bernin [b], Derek Creaser [a], Louise Olsson [a,*]

[a] Competence Center for Catalysis, Chemical Engineering, Chalmers University of Technology, Gothenburg SE 412 96, Sweden
[b] Department of Chemistry and Chemical Engineering, Chalmers University of Technology, Gothenburg SE-412 96, Sweden

ARTICLE INFO

Keywords:
Unsupported NiMoS catalysts
Kraft lignin
Hydrolysis lignin
Lignin-oils
Hydrotreatment

ABSTRACT

Catalytic hydroconversion of Kraft and hydrolysis lignins was for the first time compared in a batch reactor over an unsupported NiMoS-SBA catalyst. We also report the effect of key reaction parameters on the yields and properties of the products. The results obtained at 20 wt% catalyst loading for hydrolysis lignin showed the highest monomer yield of 76.0 wt%, which consisted of 39 wt% aromatics with the lowest alkylphenolics yield of 10.1 wt%. Identical operating conditions, 400 °C, 80 bar, 5 h at 10 wt% catalyst loading, were used to compare both lignins and the highest monomer yield (64.3 wt%) was found for the hydrolysis lignin, consisting of 16.0 wt % alkylphenolics and 20.1 wt% aromatic compounds. These values are considerably higher than those for Kraft lignin with its 47.0 wt% monomer yield. We suggest that the reason for high yields of monomeric units from hydrolysis lignin is that it is more reactive due to its lower ash and sulfur contents and the chemical structural differences compared to the Kraft lignin. More precisely, the bio-oil from hydrolysis lignin contained higher yields of small molecules, sourced from ring-opening of cellulose in the hydrolysis lignin, which could stabilize the reactive oligomeric groups. These yields were two to seven times higher from kraft and hydrolysis lignin, respectively, compared to those obtained without catalyst. The results showed that the NiMoS-SBA catalyst is a promising catalyst for reductive depolymerization of lignin and in addition that the regenerated catalyst had good stability for multiple reaction cycles.

1. Introduction

The replacement of fossil fuels is of paramount importance. For renewable energy to be sustainable, it must be limitless and provide net-zero CO_2 emissions. This demand still depends on several factors including biomass source, regional location and available technologies. Lignin, as a key component of the plant cell wall, has been identified as a major potential source of aromatic renewable resources. From an energy point of view, it has a high C/O ratio and accounts for 40 % of the carbon-based energy content in biomass [1]. However, a vast amount of generated lignin, from paper and bio-ethanol production, is predominantly incinerated and converted into heat or thermal energy and less than 2 % was sold for the production of value-added chemicals [1].

Lignin consists of polymerized three-dimensional monomers, including syringyl (S), *p*-hydroxyphenyl (H), and guaiacyl (G) units, which have been investigated as model compounds for catalytic hydroconversion [2]. The most common linkages of carbon–oxygen (β-O-4) and carbon–carbon (β-5, 5–5, β-1 and β-β) are formed from these 3D monomers, particularly from S and G monomer units. The β-O-4 bonds are the most abundant interunit linkages, making up almost 50 % of all intermonomer linkages in softwoods and 60 % in hardwoods [3]. The cleavage of two β-O-4 bonds, which are located one on each side of the aromatic unit, is required to produce one monomer unit [4]. Moreover, it has been observed that a higher S/G ratio gives a higher yield of monomers during catalytic depolymerization. It has been reported that during catalytic depolymerization at 250 °C of birch lignin (S/G = 3) a monomer yield of 50 mol % is found, whereas a poplar lignin (S/G = 1.5) produced yields of 44 mol % [5]. Interestingly, Shuai *et al.* observed a monomer yield of 78 mol % using high-syringyl transgenic poplar lignin (S/G = 38) [6].

With lignin being an integral part of the plant cell wall, its extraction is one of the challenges to achieve a suitable S/G ratio with a high quality. The extraction, depending on its process conditions, may add further structural complexity to the native physicochemical properties of the lignin. The lignin product is often contaminated or not fully extracted with a significant amount of residual carbohydrates or process

* Corresponding authors.
E-mail addresses: abdenour.achour@chalmers.se (A. Achour), louise.olsson@chalmers.se (L. Olsson).

https://doi.org/10.1016/j.cej.2022.139829

Available online 19 October 2022

chemicals [7]. These challenges have created ambiguities to understand the structural composition of lignin, and hence their chemical reaction network during the depolymerization of processed lignins. Consequently, identifying practical extraction and pretreatment conditions yielding a high quality lignin suitable for facile depolymerization requires further attention and development [2,7,8].

Numerous approaches and methodologies have been investigated for Kraft lignin depolymerization. The catalytic reductive depolymerization with hydrogen has been studied extensively as a means to liquify Kraft lignin and selectively produce monomers. Typically, conventional hydrotreating catalysts based on supported molybdenum sulfides (MoS_2), promoted by cobalt (Co), nickel (Ni) or iron (Fe) have been studied [9,10]. Recent studies of these transition metal based catalysts showed that they exhibited high activity and selectivity for the C—O bond cleavage [1,11,12]. However, the sulfate pulping process contributes to high ash and sulfur contents in Kraft lignin [13]. The major problem, along with the coke deposition via bimolecular condensation reactions, is that inorganic contaminants can lead to catalyst deactivation during the catalytic depolymerization of Kraft lignin [14].

Compared to Kraft lignin, hydrolysis lignin, containing less ash and sulfur, can be produced from conversion of lignocellulosic biomass during enzymatic hydrolysis, which results in solid lignin (≥60 wt%), and unreacted cellulose [15]. However, limited studies have investigated catalytic reductive depolymerization of enzymatic hydrolysis lignin. Tymchyshyn *et al.* used a MoRu/AC catalyst to depolymerize hydrolysis lignin in acetone solvent and obtained low molecular weight bio-oils (380 g/mol) with high yields of around 85 wt% at 340 °C [15]. It was also reported that an aromatic monomer yield of 12.1 wt% was obtained for hydrolysis lignin over a 5 wt% Ni/AC catalyst at 240 °C for 4 h with 30 bar H_2 in methanol [16]. Bai *et al.* used 15 wt% Ni/Al_2O_3 to depolymerize hydrolysis lignin and obtained a yield of 10.3 wt% of aromatic monomers at 320 °C after 7.5 h under 28 bar H_2 in ethanol [17]. The effect of reaction conditions on the depolymerization of hydrolysis lignin has been investigated in a semi-continuous process over a sulfided NiMo/γ-Al_2O_3 catalyst [18]. A full conversion was achieved and the liquid products, mainly aromatics, naphthenes, and phenols increased under the severe reaction conditions of 380 °C, and 70 bar H_2. Recently, Sang *et al.* examined the depolymerization of hydrolysis lignin over an unsupported Ni catalyst in supercritical ethanol and achieved complete liquefication, with the highest monomer yield of 28.9 % at 280 °C for 6 h with 20 bar H_2 [19]. Importantly, these unsupported catalysts decrease the mass transfer limitations inherent to supported catalysts, to achieve a more complete liquefication and prevent char formation during the depolymerization [19]. More recently, the direct conversion of hydrolysis lignin into cycloalkanes over a NiMo/γ-Al_2O_3 catalyst was carried out in a single step at 320 °C for 7.5 h [20]. The highest obtained overall yield of cycloalkanes was 104 mg/g enzymatic hydrolysis lignin, with a ethyl-cyclohexane selectivity of 44 wt% [20].

However, there are to the best of our knowledge, no published studies where the efficiency of catalytic valorization in reducing conditions have been compared using Kraft and hydrolysis lignin, which is the objective of the current work. In this work, we introduce a facile preparation method for an unsupported NiMoS catalyst that is highly active with a high surface area. This catalyst can be a key factor in enhancing the hydrodeoxygenation and hydrogenation capabilities, and simultaneously decreasing the unwanted repolymerization reactions producing char. In addition, the reaction pathways for both lignins are proposed and discussed to reveal the key steps in their depolymerization and how they differ.

2. Material and methods

2.1. Feedstocks and chemicals

Two different lignins were investigated. Kraft lignin is a three-dimensional polymer that has undergone a hydrolytic degradation process [21,22]. It was supplied by Sigma-Aldrich as a brown dry powder. The enzymatic hydrolysis lignin was kindly provided by Sekab (Sweden). Prior to all experiments, the lignin samples were dried at 80 °C in an oven. The chemicals used were of analytical grade and were not further purified. The reagents used can be found in Supplementary Information (SI).

2.2. Catalyst synthesis

Unsupported $NiMoO_4$ catalysts were synthesized by a nanocasting method using mesostructured silica as a hard template. SBA-16 and MCM-41, consisting of only silica, were used as templates. Hard templating is an important strategy to synthesis crystalline mesoporous materials. The unique structure of the hard template restricts the crystallization or aggregation of the precursors, and a mesoscopic phase having a structure opposite to that of the template can be obtained with the removal of template material by the appropriate method [23]. A mixture of ammonium heptamolybdate tetrahydrate and nickel nitrate hexahydrate, in a molar ratio of 1:1, was dissolved in ethanol. The aqueous mixture was added to the mesoporous silica and stirred for 2 h at room temperature. Subsequently, ethanol was evaporated gradually using a water bath at 65 °C. The obtained paste was then calcined at 200 °C for 6 h. The resulting solid was re-impregnated again, followed by calcination at 450 °C for 6 h at a heating rate of 6 °C/min. Lastly, the silica template was removed from the mesoporous composite by 0.5 M NaOH using a vacuum filtration process. The solid products were washed with deionized water several times and then dried at 110 °C. Elemental analysis using ICP confirmed the absence of templates and showed the successful removal of the template. The absence of silica was also confirmed with XPS, XRD and TEM-EDS. The oxide forms of the unsupported catalysts will be denoted NiMo-SBA and NiMo-MCM, respectively, according to the mesostructured SBA-16 and MCM-41 templates used in their synthesis.

2.3. Catalyst characterizations

Elemental composition of the catalysts was determined by using an inductively coupled plasma (ICP) and was performed by ALS Scandinavia AB after digestion of the solids in an acid solution.

Powder X-ray diffraction (XRD) was used to examine the crystallinity of the catalysts. This was done using a Bruker D8 Advance (40 kV; 40 mA; Cu Kα radiation (λ = 1,542 Å); 2θ range of 20-80°; 1°/min scan speed). The textural properties of the samples, such as pore volume, surface area and pore size were determined by nitrogen physisorption using a TriStar 3000 analyzer. Prior to N_2-physisorption measurements, approximately 300 mg sample was degassed overnight at 300 °C under a continuous flow of nitrogen gas. After drying, the N_2-physisorption isotherms were collected at −195 °C under vacuum. The specific surface area and pore size were determined using the Brunauer-Emmett-Teller equation (BET) and the Barret – Joyner – Halenda equation (BJH), respectively.

The lignins and catalysts were thermally characterized by TGA with a TGA/DSC 3+ Star system (Mettler Toledo, Switzerland) featuring automated temperature and weight control as well as data acquisition. The samples were analyzed, without any pre-treatment, from 25 to 800 °C (to 900 °C for catalysts) with a 5 °C/min heating rate. Dry air and nitrogen were used as carrier gases for comparison.

Scanning electron microscopy (SEM) was used to study the surface structure and morphologies of the sulfided catalyst samples with a JEOL JSM6400, operating at 25 kV. The shape and size of the metal species in the catalysts were examined using transmission electron microscopy (TEM), with a FEI Titan 80–300 microscope (field emission gun; a probe Cs corrector; Gatan image filter Tridium; 300 kV). X-ray photoelectron spectra of the fresh sulfided catalyst was recorded using a PerkinElmer PHI 5000 Versa Probe III scanning XPS Microprobe apparatus equipped with a monochromatic Al Kα source with a binding energy of 1486.6 eV

and the beam size diameter of 100 μm. The reference used is so-called adventitious carbon (AdC) using the C 1 s peak from the surface contamination layer and its binding energy (BE) is set to 284.6 eV.

The NH_3 temperature-programmed desorption (NH_3-TPD) experiments were conducted in a Differential Scanning Calorimeter (DSC, Setaram Sensys), where the gas flow was regulated with mass flow controllers (MFC, Bronkhorst), and the outlet gases detected with a mass spectrometer (MS, Hiden Analytical HPR 20). 50 mg of $NiMoO_4$ and NiMoS unsupported catalysts were pre-treated at 400 °C for 2 h in an argon flow of 20 mL/min. This was followed by exposing the catalyst to 4 vol% NH_3 in Ar (10 mL/min) for 2 h at 120 °C. Thereafter the catalyst was flushed with Ar for 6 h and then the NH_3 desorption was studied while increasing the temperature from 120 to 700 °C at a ramp rate of 5 °C/min.

2.4. Analytical methods for products

Elemental analyses (EA) were performed to determine the C, H, N, and S content in the feed lignins, and lignin oils using a vario MICRO cube analyzer. The MICRO cube analyzes the CHNS content of organic compounds in one single run. The amount of oxygen was determined by difference from the CHNS content. All analyses were performed twice and the average value is given.

The water content in organic samples was determined by Karl Fischer (KF) titration using a Metrohm Titrino 807 titration equipment. The sample was added to a glass container with Hydranal® (Riedel de Haen) and the titrations were performed with Karl Fischer titrant Composite 5 K (Riedel de Haen). All analyses were performed twice, and the average value is given.

^{31}P NMR technique was used for the characterization and quantification of hydroxyl and carboxylic acid groups in lignin oils using an earlier method involving a prior derivative phosphitylation step [24]. The amount of different hydroxyl groups (mmol OH/g) in lignin oil samples was calculated according to [24]. The ^{13}C solid-state NMR was conducted on a Bruker Avance III 500 MHz spectrometer equipped with a 4 mm MAS BB/^1H probe. The rotor was spun at 10 kHz and a cross-polarization time of 1.5 ms was used.

The GC-TCD technique was used to characterize gases formed during lignin hydroconversion. The gas samples were analyzed by a calibrated GC (450-GC, Varian) that was equipped with a TCD detector. A GS-GASPRO column (30 m, 0.32 mm) was used to separate and quantify the concentration of H_2, CO, CO_2, CH_4, and C_2+ light hydrocarbons. The quantification was performed from the calibration of each gas using reference mixtures. All measurements were carried out in triplicate and the average value is provided.

GCxGC-MS analysis was performed on organic liquid samples using an Agilent 7890B apparatus equipped with a closed cycle cryogenic jet modulation (ZX2 Model) from Zoex Corporation, two parallel detectors, an FID and a quadrupole MSD, and two columns. The first column was a moderately polar VF1701ms column (30 m × 0.25 mm × 0.25 μm) and the second column was a nonpolar DB-5 MS UI column (1.2 m × 0.15 mm × 0.15 μm). The temperature of the injector port and MS interface were set at 250 °C. The column flow was set at 0.8 mL/min. The oven temperature program was set initially at 40 °C and held for 1 min, then heated up to 280 °C at 3 °C/min. The modulation time was 6 s. The data was processed via GC image 2.5 (Zoex Corporation) using GC Project and Image Investigator functions. The 2014 NIST library (Match Factor >700), together with high resolution mass spectral data, were used for compound identification. To assess the relative standard deviation of each analysis, an internal standard was loaded before analysis by GCxGC. From GC Image Investigator, the relative standard deviations (RSD) in the first-dimension retention time, the second-dimension retention time and peak volume were less than 0.1 %.

2.5. Reaction experiments and separation protocol

The hydroconversion experiments were carried out in a 450 mL stainless-steel Parr reactor. The influence of catalyst loadings (ranging from 5 to 20 wt% based on a constant 5 g of dry lignin always loaded into reactor), pressures (50–80 bar H_2) and temperatures (330–400 °C) have been investigated (Table 1). In a typical experiment, the reactor was loaded with catalyst and lignin (5 g) in 70 mL of hexadecane as a co-processing solvent to reduce the exothermic heat effects. To create a baseline for the study, reaction experiments using only hexadecane with lignin were included in the experimental plan. The sulfidation of the $NiMoO_4$ catalyst was performed in-situ in the liquid phase, with the lignin feedstock and with the addition of (0.25–0.75 mL) dimethyl disulfide (DMDS). In-situ sulfidation of the unsupported $NiMoO_4$–SBA was carried out simultaneously with hydroconversion of Kraft and hydrolysis lignins. The advantage of in-situ activation is the simplification of the startup procedure. The amount of DMDS added depends on the catalyst amount used. During the sulfiding step for all experiments, a mixture of lignin, catalyst, and solvent were blended. Meanwhile, a small amount of DMDS (250, 500 or 750 μL) was added to the corresponding reaction mixture to maintain the sulfidity of the catalyst (5, 10 or 20 wt%, respectively). Under identical operating conditions, some experiments were performed to compare products yields from in-situ sulfided versus pre-sulfided $NiMoO_4$..

After the reactor was closed, it was flushed for 3–5 times with nitrogen to remove the air and thereafter purged three times with hydrogen. After leak testing, the reactor was initially pressurized with 16–25 bar H_2 (depending on the target pressure for reaction conditions) and heated up to the designated temperature at an approximate heating rate of 5 °C/min while stirring at 1200 rpm. The time zero was set once the desired reaction temperate and pressure were reached. In the case of our study, duplicate reaction experiments were repeated for many of our experiments and the relative standard deviation (%, RSD) was determined to be within 9.0 %.

After each experiment, different fractions of lignin products were recovered and analyzed. The typical products are gas, liquid bio-oil, unconverted lignin and solid char, as depicted in the product recovery protocol (Fig. S1, Supplementary Information (SI)). The pressure was recorded after the reactor was cooled to room temperature. The hydrogen consumption was determined from the difference in the initial and final pressures at room temperature [25,26]. Hydrogen was considered as an ideal gas and other gases produced during the reaction, were accounted for in the calculation of the hydrogen consumption. The pressure was released to atmospheric pressure and the gas products were collected in a 1 L Tedlar gas bag to determine its composition by using

Table 1
Catalytic hydrotreatment Operational Conditions. In all experiments 5 g of dry lignin was used and 70 mL of hexadecane was added as a solvent.

Experiments Notation	Operating Conditions Lt[a]—T[b]—P[c]—t[d]—W[e]
Kraft Lignin	
KES_0	KL–400–80–5–W_0
KES_1	KL–330–50–5–W_5
KES_2	KL–400–50–5–W_5
KES_3	KL–400–50–12–W_5
KES_4	KL–400–80–5–W_5
KES_5	KL–400–80–5–W_{10}
Hydrolysis Lignin	
HES_6	HL–400–80–5–W_0
HES_7	HL–400–80–5–W_5
HES_8	HL–400–80–5–W_{10}
HES_9	HL–400–80–12–W_{10}
HES_{10}	HL–400–80–5–W_{20}

[a] indicates Lignin type: Kraft (KL), Hydrolysis (HL), [b] Temperature applied (°C), [c] Pressure applied (bar), [d] residence time (hrs.), and [e] wt.% of catalyst loaded based on 5 g of dry lignin.

Table 2
Pore structural parameters of the unsupported catalysts synthesized using different hard templates.

Catalysts	S_{BET} [a] ($m^2 \cdot g^{-1}$)	V_{mes} [b] ($cm^3 \cdot g^{-1}$)	d_{BJH} [c] (nm)
$NiMoO_4$-SBA (as prepared)	155	0.19	5.0
NiMoS-SBA (pre-sulfided) *	53	0.08	5.9
$NiMoO_4$-MCM (as prepared)	207	0.61	11.8

[a] Calculated by the BET method.
[b] The total pore volume was obtained at a relative pressure of 0.99.
[c] Mesopore diameter was calculated using the BJH method. Pore morphology: NiMo-SBA cubic, NiMo-MCM hexagonal.
* NiMoS-SBA pre-sulfided under 330 °C, 20 bar H_2 for 2.5 h.

GC-TCD. The blended organic product was recovered, filtered and labelled as lignin oil. Subsequently, the reactor was rinsed with acetone, filtered, and this product fraction was labelled as the acetone soluble phase. Moreover, the solid phase (char, unconverted lignin, and catalyst) was washed with acetone to remove any adsorbed organics.

The unconverted lignin was determined by suspending 0.5 g of solid residue in 15 mL of DMSO and thereafter stirring for 24 h at room temperature. After filtration of the solution, the solids were washed with acetone and dried. The weight difference between the solids before and after the washings was assumed to be the weight of unconverted lignin. The conversion, char, and monomer yields were determined using Eqs. (1) to (3).

$$\text{Conversion (wt.\%)} = \frac{\text{initial lignin feed (g)- unconverted lignin (g)}}{\text{initial lignin feed (g)}} \text{ x } 100 \quad (1)$$

$$\text{Char yield (wt.\%)} = \frac{\text{(solid fraction (g))-(unconverted lignin (g) + catalyst (g))}}{\text{initial lignin feed (g)}} \text{ x } 100 \quad (2)$$

$$\text{Monomer yield (wt. \%)} = \frac{\text{monomer (g)}}{\text{initial lignin feed (g)}} \text{ x } 100 \quad (3)$$

3. Results and discussions

3.1. Characterization of the unsupported catalysts

The elemental composition was measured using ICP and the unsupported $NiMoO_4$-SBA catalyst had a Mo/Ni ratio of 1.08). The pore structural parameters are summarized in Table 2, which displays high surface areas in the range of 155–207 m^2/g for none sulfided catalysts. A sulfidation treatment of the unsupported $NiMoO_4$-SBA leads to an inevitable decrease of the catalyst surface area from 155 to 53 m^2/g and a pore volume decreased from 0.19 to 0.08 $cm^3\ g^{-1}$, which may be due to the inclusion of sulfur to form NiS_2 and MoS_2 new phases. These catalysts exhibit the type-IV isotherm, confirming their ordered mesostructured morphology. Moreover, the pore size distributions correlate with those of the templates used and exhibited a narrow pore size distribution at around 5 nm for both as prepared and pre-sulfided catalysts. While using MCM-41 as a template, relatively larger cages and mesoporous channels, corresponding to the MCM-41 template, were observed. The pore diameter of the unsupported $NiMoO_4$-MCM catalyst enlarged to 11.8 nm with a significantly larger pore volume of 0.61 $cm^3\ g^{-1}$.

The crystal structures of the unsupported $NiMoO_4$ were characterized by XRD (Fig. 1). The broad peaks indicate a small crystallite size of the samples. Comparison of the $NiMoO_4$ fabricated via the two different hard templates, SBA and MCM, reveals that there are distinct differences in the XRD patterns (Fig. 1a). α-$NiMoO_4$ and β-$NiMoO_4$ phases have a monoclinic crystal structure (group space C12/m1). The characteristic peak of the β phase is $2\theta = 26.4°$ and for the α phase it is $2\theta = 28.7°$. From the structural point of view, the relevant important differences between both phases are the molybdenum ion coordination in the crystal structure, being octahedral clusters, [MoO_6], for the α-$NiMoO_4$ and tetrahedral [MoO_4], for the β-$NiMoO_4$ powder [27]. It has been found that for the preparation of highly active unsupported NiMo catalysts, the β-$NiMoO_4$ phase is most favorable for hydrodesulfurization (HDS) reactions [28–31]. In this work, the unsupported $NiMoO_4$ fabricated from the SBA hard template which exhibited the β-$NiMoO_4$ phase was

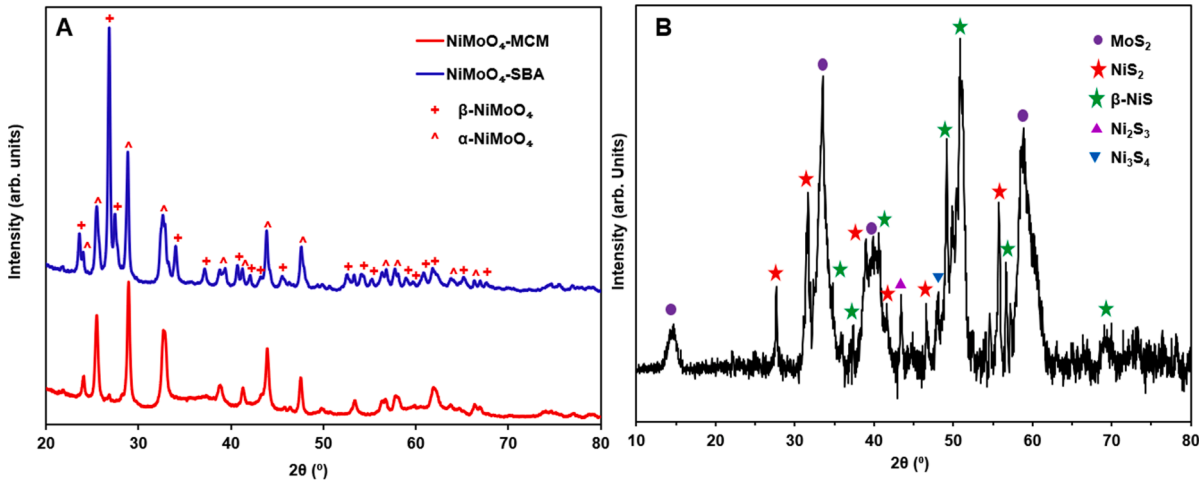

Fig. 1. XRD of the as-prepared unsupported $NiMoO_4$ powders using different hard templates MCM and SBA (a) and the pre-sulfided unsupported $NiMoO_4$-SBA (b).

therefore selected for the catalytic hydroconversion.

The XRD patterns of the pre-sulfided $NiMoO_4$-SBA are depicted in Fig. 1b. The sulfided NiMoS showed strong diffraction peaks consistent with the relatively good crystalline structure of MoS_2 (JCPDS-ICDD 371492), NiS_2 (JCPDS-ICDD 89–3058), and β-NiS (JCPDS-ICDD 12–0041). The presence of peaks at 2θ value of 14.5, 33, 39 and 59 corresponded to the (002), (100), (103) and (110) planes of MoS_2 [32]. As revealed by the XRD patterns, peaks due to NiS_2 and β-NiS species were also detected. Some peaks at 2θ value of 27, 31, 35, 38, 45, and 53 were observed, matching well with the NiS_2 [33]. Moreover, the presence of peaks can be clearly indexed to β-NiS at 2θ value of 33, 37, 41, 49, 51, and 57 corresponding to (300), (220), (221), (131), (410) and (330) planes [34]. Obvious diffraction peaks from other compounds, such as Ni_3S_2 and Ni_3S_4, were also observed at 2θ value of 43.5, and 48 respectively [35,36]. No obvious ternary Ni-Mo-S and $NiMoO_4$ oxide patterns were observed. It is noteworthy to mention that before XRD analysis, the pre-sulfided catalyst was passivated under a flow of 25 mL/min of 2 % O_2 in Ar for 2 h and thereafter transferred into another N_2 atmospheric bottle to avoid air contact.

The SEM image of the sulfided NiMoS-SBA catalyst showed two major structural features (Fig. S2a, SI). Small pore sizes can be seen in the material with an average pore size of 5–10 nm (white insert). These smaller pores are the fine intra-aggregate pores of the material. The larger sized pores (>50 nm) may be attributed to the secondary pores formed by the combination of primary particles. The TEM result of the freshly sulfided NiMoS-SBA catalyst is given in Fig. S2b (SI). Areas with black thread-shape fringes that have spacings of about 0.5 nm indicate a high purity of the active components and are characteristic of the (002) basal planes of crystalline MoS_2 (XRD pattern Fig. 1b). This has been confirmed by Yoosuk et al. [37]. As well-known from the intercalation model, slab growth occurs in parallel and perpendicular directions [2]. But for NiMoS in Fig. S2b, the slabs seem curved. These results are in good agreement with the recent study of Yoosuk et al. [37], who also suggested a reduction in the slab length and form when Ni was incorporated into the Mo sulfide. In these directions, the promoting Ni atoms are bonded (in intercalation positions) by Van der Walls forces [36]. It is generally accepted that the best hydrotreating MoS_2 catalysts are promoted with Ni or Co atoms located at the edges of MoS_2 slabs [2], which is discussed later in connection to the lignin depolymerization. In good agreement with the literature data, it can be assumed that the formation of Ni_xS_y active sites occurred at the rims of MoS_2 sheet crystals.

Fig. 2 displays the TGA and DTG profiles of the pre-sulfided and as prepared unsupported $NiMoO_4$-SBA catalysts. For the unsulfided $NiMoO_4$-SBA catalyst, it shows two weight loss areas, totaling about 6.4 wt% up to the reaction temperature of 400 °C, together with corresponding endothermic peaks (Fig. 2b). The first weight loss was about 3.4 wt% from 75 to 170 °C, based on a calculation of the first derivative of the weight loss curve at 70.4 °C and might be attributed to the loss of physically absorbed and chemically bonded water. The following weight loss was about 3.0 wt% from 210 to 415 °C, which can be due to the total phase transformation of α-$NiMoO_4$ (octahedral MoO_6) to pure β-$NiMoO_4$ (tetrahedral MoO_4) above 286 °C, which was reported by Pillay et al. by measuring the XRD pattern at high temperature to characterize the α-$NiMoO_4$ and β-$NiMoO_4$ phase transitions [38].

After the sulfidation of the unsupported $NiMoO_4$-SBA catalyst, the TGA thermogram showed a 6.5 wt% weight loss up to 400 °C, which was similar as for the unsulfided $NiMoO_4$-SBA. Besides, it also shows two endothermic weak peaks (pre-sulfided NiMoS, Fig. 2b) that may refer to a decomposition of the α-$NiMoO_4$ and β-$NiMoO_4$ formed due to oxygen contact. At higher temperature, a weight loss was observed from 400 to 650 °C and thereafter another weight loss a higher rate in the 650–900 °C range. It is likely that these weight losses are originating from decomposition of different sulfur species on the catalyst since they were not found on the non-sulfided catalyst (Fig. 2b, blue line).

In order to investigate the nature of the surface species, XPS analysis of the sulfided catalyst was conducted and shown in Fig. 3. Based on XPS analysis, the atomic percentage of various elements present at the surface of the catalyst is given in Table 3. Note that the sulfided sample could be partially oxidized due to oxygen contact when storing and transferring the sample to the XPS instrument, which could possibly explain the high oxygen content (Table 3). XPS was used to investigate the chemical states of Mo, Ni and S in the pre-sulfided NiMoS, shown in Fig. 3. The XPS spectra showed that the binding energies of Mo $3d_{5/2}$ and Mo $3d_{3/2}$ were located at 228.7 eV and 232.1 eV respectively, owing to the Mo^{4+} in MoS_2 [39,40] and there is also a weak peak located at 235.2 eV assigned to Mo^{6+} $3d_{5/2}$ of MoO_3 formed due to oxidation of Mo (Fig. 3b). Another weak peak at the binding energy at 225.9 eV is ascribed to S2s of S_2 in MoS_2 [39,40]. Besides, there are two strong peaks at 161.5 and 162.7 eV in the S2p spectrum (Fig. 3c), which are assigned to the $S2p_{3/2}$ and $S2p_{1/2}$ binding energies for S^{2-} of MoS_2 and NiS_2. Moreover, there are three peaks present in the Ni 2p spectrum (Fig. 3d) at 853.3, 856.4, and 861.7 eV, which could be assigned to NiS_2, nickel

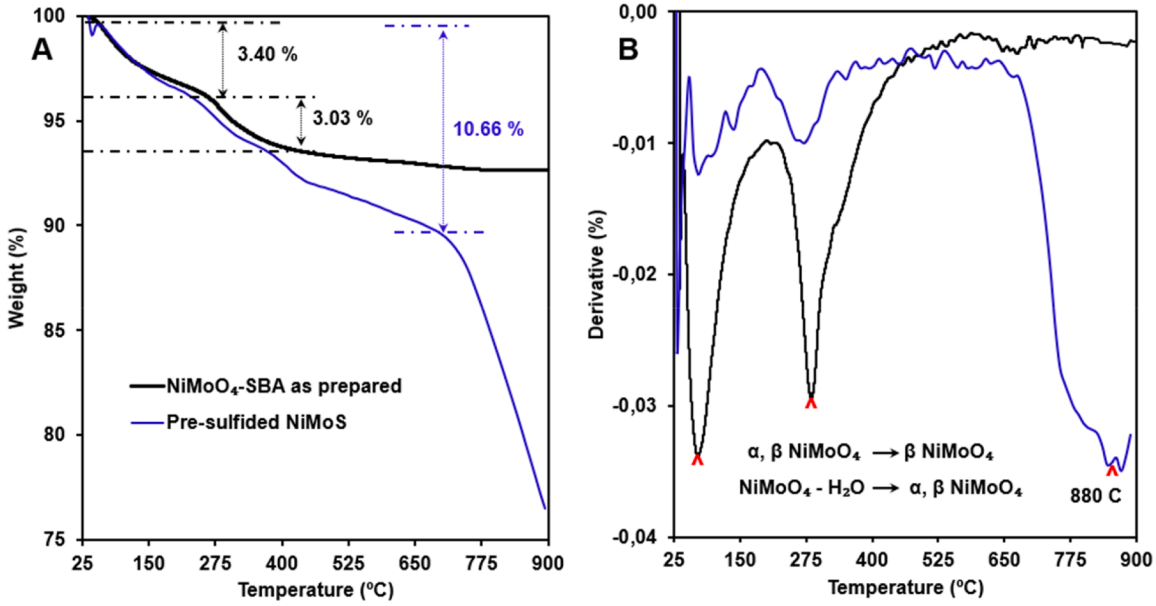

Fig. 2. (a) Thermogravimetric analysis (TGA) and (b) Derivative thermogravimetric (DTG) curves of the pre-sulfided and as-prepared $NiMoO_4$-SBA.

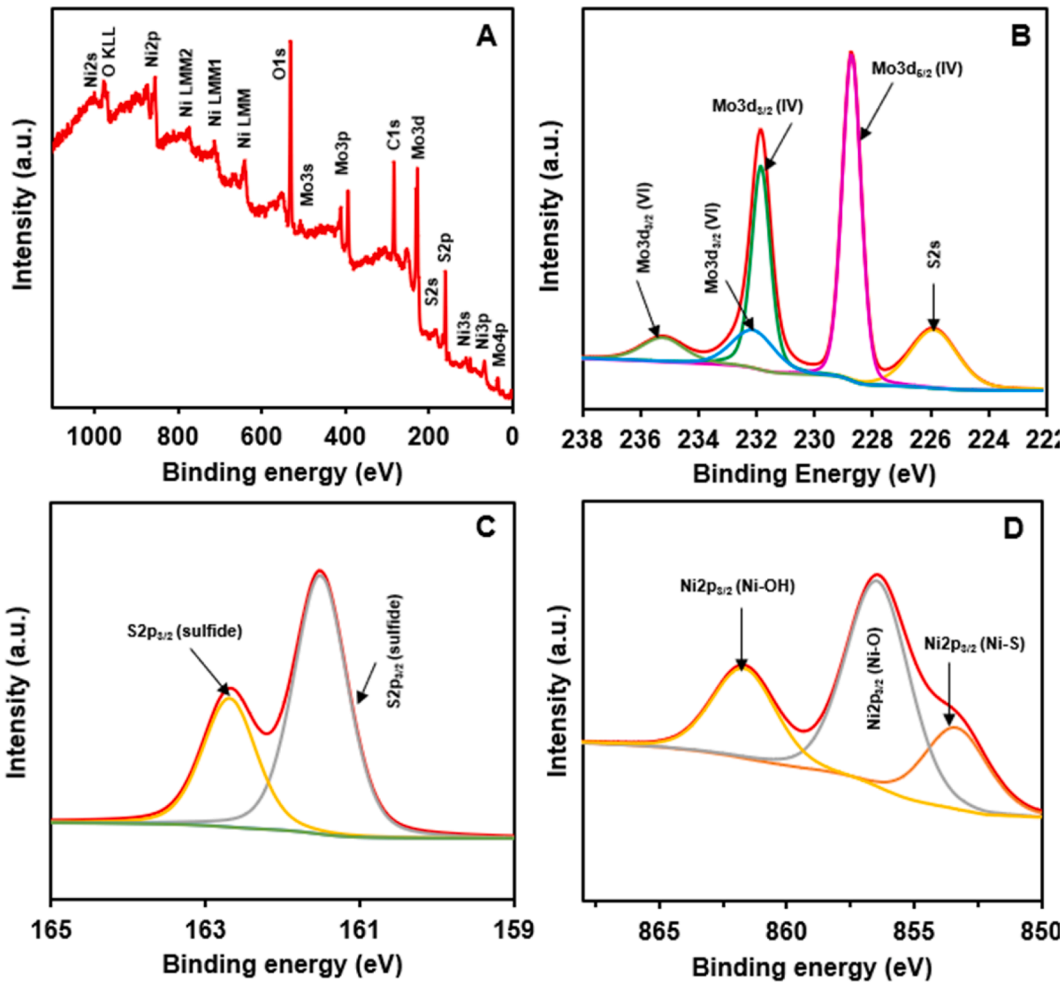

Fig. 3. XPS spectra of pre-sulfided NiMoS-SBA. (A) full scan spectrum of NiMoS, with high resolution spectra of (B) Mo3d, (C) S2p, and (D) Ni2P.

Table 3
Atomic and molar percentage of various elements present in pre-sulfided $NiMoO_4$-SBA catalyst using XPS analysis.

Elements	C1s*	O1s**	S2p	Ni2p	Mo3p	Ni/(Ni + Mo)
Atomic %	36,4	34,9	14,6	6,3	7,7	0.45
Molar	16.9	21.7	18.1	14.4	28.9	0.33

Note: *AdC contamination layer. ** note that the samples were stored in air prior to XPS measurements.

oxide and nickel hydroxide, respectively [36,40].

NH_3-TPD profiles of $NiMoO_4$-SBA and NiMoS-SBA catalysts are presented in Fig. S3 (SI) to evaluate their surface acidity. Both catalysts exhibited moderate (200–400 °C) and strong (>400 °C) acid sites. The NH_3-TPD profile of $NiMoO_4$-SBA displayed a relatively wide peak at 300 °C and a minor peak at 550 °C, which were attributed to moderate and strong acid sites, respectively. Whereas after sulfidation, it can be observed that there is an important decrease in the number of moderate acid sites, while an increase in the acid strength for sulfided NiMoS-SBA.

3.2. Characterization of lignins and product recovery

3.2.1. Lignin characterization

Chemical structures and thermal characterization of lignins were carried out through thermo-gravimetric analysis (TGA), differential scanning calorimetry (DSC), elemental analysis (CHONS), and solid state ^{13}C NMR. TGA curves, under oxidizing atmosphere (Fig. 4),

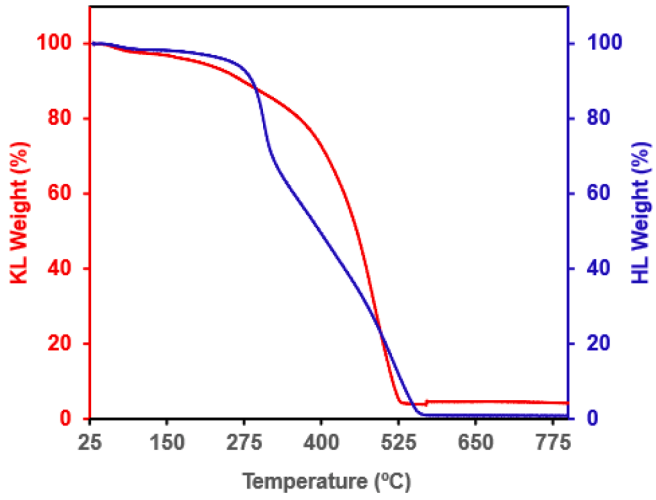

Fig. 4. TGA curves of the kraft (red line) and hydrolysis lignins (blue line) under oxidizing atmosphere. (For interpretation of the references to colour in this figure legend, the reader is referred to the web version of this article.)

showed that the water content corresponds to the weight loss of about 2.3 wt% for Kraft lignin and 1.5 wt% for hydrolysis lignin at 100 °C, whereas the remaining weight at the end corresponds to the ash content of 3.5 wt% for Kraft lignin and only 0.5 wt% for hydrolysis lignin. Elemental CHONS analyses, ash, water content as well as the H/C and

Table 4
Elemental analyses, ashes, water, and H/C and O/C ratios and HHV for the lignins.

Wt.%	Kraft Lignin	Hydrolysis Lignin
C	61.2	55.9
H	5.6	5.7
O	30.5	38.1
N	0.3	0.3
S	1.4	0.1
Ashes	3.5	0.5
Water	2.3	1.5
Total	104.8	102.1
Atomic ratio		
H/C	1.1	1.3
O/C	0.4	0.5
HHV (Mj/Kg)*	24.7	22.3

* Higher Heating Value.

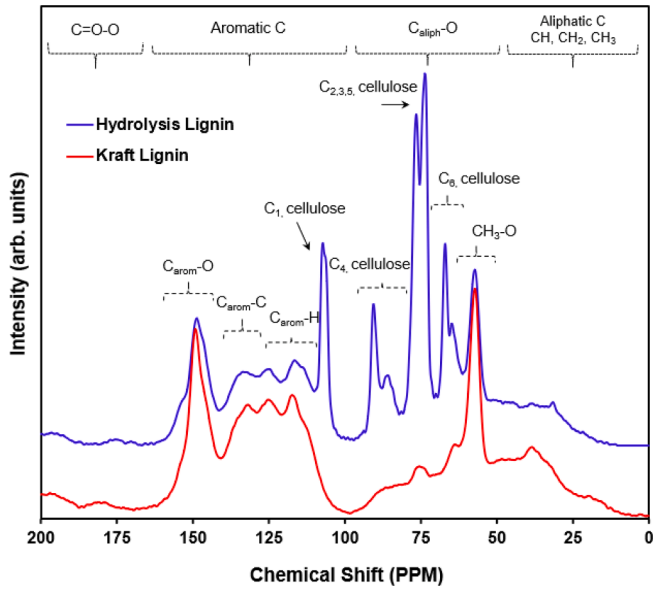

Fig. 5. Solid state 13C NMR spectrum of Kraft and hydrolysis lignins.

O/C atomic ratios are reported in Table 4.

The chemical structures of Kraft and hydrolysis lignin were analyzed by means of solid-state ^{13}C NMR (Fig. 5). Both lignins showed small signals in the area 200–160 ppm, indicating a low amount of C═O structure, attributed to C═O bonds in Ar-CHO or R-O-CO-CH_3 at 177.5 ppm and 181 ppm, respectively [41]. In the C_{arom} region (110–150 ppm), the intense peak at 150 ppm corresponds to C_{arom}-O, whereas three weak signals were observed at 115, 123 and 127 ppm corresponding to C_{arom}-C and C_{arom}-H [42,43]. The ^{13}C NMR spectrum of hydrolysis lignin showed characteristics of typical lignocellulosic biomass, which is primarily composed of cellulose (62–110 ppm) and lignin [44]. Fu *et al.* showed that hydrolysis lignin is covalently attached onto cellulosic moieties, indicating that the cellulose from lignocellulosic biomass is not fully isolated [15,45–47]. Note that the high O elemental content result for hydrolysis lignin (38.1 wt%) may be partly due to the presence of cellulosic oxygen content. Moreover, methoxy groups were detected at 58.0 ppm for both lignin types. The CH, CH_2, and CH_3 saturated aliphatic signals (<50 ppm) could not be clearly observed and distinguished. Some identical peaks were observed in both lignins, but the peak intensities were higher for Kraft lignin than the hydrolysis lignin. By comparing these different analytical results, we can observe that both lignins are connected randomly through β-β or β-aryl ester, G-type β-O-4 and β-5 linkages, and cellulosic units for hydrolysis lignin.

TGA and DSC curves for hydrolysis and Kraft lignin under inert atmosphere are given in Fig. 6. TGA analysis showed that Kraft and hydrolysis lignins start to decompose in the range of 175–460 °C and 250–405 °C, respectively. Thus, reactions involving lignins are already expected to take place to a certain extent when heating up the reactor to the final chosen temperature, in our case 400 °C [48]. Moreover, under inert atmosphere at 550 °C, the char yields of Kraft (43 wt%) and hydrolysis lignin (31 wt%) were higher than in an oxidizing environment (see Fig. 4 and Fig. 6). These results show that depolymerization of

Table 5
Summary of thermal and catalytic hydrotreatment experiments.

Entry	Operating Conditions	Conv. (Wt. %)	Oil Yield (Wt. %)	Gas Yield (Wt. %)	Char Yield (Wt. %)	Water Yield (Wt.%)
Kraft Lignin						
KES_0	KL–400–80–5–W_0	98.9	45.3	0.3	52.9	0.7
KES_1	KL–330–50–5–W_5	99.5	48.7	0.1	40.5	0.3
KES_2	KL–400–50–5–W_5	91.0	49.7	2.9	30.0	2.3
KES_3	KL–400–50–12–W_5	93.0	59.2	5.6	27.0	7.9
KES_4	KL–400–80–5–W_5	95.3	61.5	2.4	29.0	4.8
KES_5	KL–400–80–5–W_{10}	91.4	65.1	2.1	20.6	4.3
Hydrolysis lignin						
HES_6	HL–400–80–5–W_0	96.6	56.4	0.7	38.6	1.6
HES_7	HL–400–80–5–W_5	97.6	76.4	3.1	14.6	6.6
HES_8	HL–400–80–5–W_{10}	94.4	83.7	1.2	8.3	2.5
HES_9	HL–400–80–12–W_{10}	95.7	86.8	2.6	3.9	5.3
HES_{10}	HL–400–80–5–W_{20}	94.9	87.1	1.0	4.6	2.6

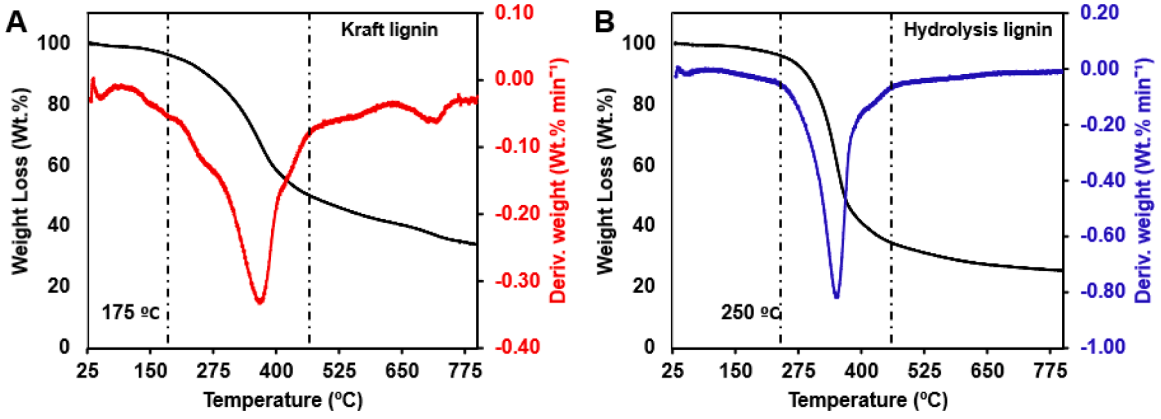

Fig. 6. TGA and derivative curves of (a) Kraft lignin; (b) hydrolysis lignin under N_2 atmosphere.

lignin without a catalyst to facilitate hydrogenation and deoxygenation reactions, is likely to yield a high char formation, particularly for Kraft lignin. It can also be seen that the thermal properties of the lignin depend on their source due to their structural variations. However, under catalytic hydroconversion, the conversions of the Kraft and hydrolysis lignins were found to be higher than 90 %, which was confirmed by performing DMSO extraction of the unconverted lignin. In the subsequent sections, we examine and discuss in detail the individual product yields of the hydrotreated lignins.

3.2.2. Hydrotreatment product distributions

For each lignin, the results of non-catalyzed and catalyzed hydrotreatment reactions are presented in Table 5. The conversions of both lignins were in the range of 91.0–99.5 wt%. The lowest lignin-oil yields were observed for the non-catalyzed experiments (KES_0, and HES_6), which correlate well with the least water content formed upon the reaction (0.3 and 0.7 wt%) and the highest char formation (52.9 and 38.6 wt%), showing a low degree of deoxygenation without the catalyst. These results also provide clear evidence that thermal depolymerization reactions play a role. Interestingly, the hydrolysis lignin results in significantly less char for uncatalyzed reactor experiments than Kraft lignin, which is consistent with the TGA results in Fig. 6. When the unsupported NiMoS-SBA catalyst (in situ sulfided) was used under the same conditions, the lignin-oil yield increased to 65.1 and 83.7 wt%, whereas the char yields were repressed to 20.6 and 8.3 wt% for Kraft (KES_5: 400 °C, 80 bar H_2, 10 % catalyst, 5 h) and hydrolysis lignin (HES_8: 400 °C, 80 bar H_2, 10 % catalyst, 5 h), respectively. The characterization results demonstrated that the sulfided catalyst had two separated sulfide phases rather than a trinary Ni-Mo-S phase. Thus, the presence of both phases of MoS_2 and Ni_xS_y likely improved the lignin conversion. This is mainly due to a synergism between Ni_xS_y and MoS_2, evidently reflected by the major XRD peaks of pre-sulfided $NiMoO_4$-SBA (Fig. 1b). Moreover, the XPS analysis confirms the presence of both phases. It was also reported by Wang et *al.* that a synthesis of NiS_2/MoS_2 has higher surface area, resulting in the exposure of more active sites [49]. The hydrodeoxygenation activity is considered enhanced in the presence of both NiS_2 and MoS_2 which could be described by a Remote Control (RC) model via hydrogen spillover [49]. According to the RC model the two separated sulfide phases of the catalyst are described as a donor phase (promoter, NiS_2) and an acceptor phase (active component, MoS_2), and thus spillover hydrogen was created on NiS_2 which then migrated to MoS_2 [49]. It was also reported that a Ni-Mo binary sulfide phase is more active than either of the single Mo or Ni sulfide phases and the maximum synergy depends on Ni/(Mo + Ni) ratio to achieve a well dispersed active phase [37].

A comparison is made between pre-sulfidation and in-situ sulfidation method (see Table S1) and it is found that both methods give similar results. Based on these results, we consider that the DMDS added was adequate to activate both in-situ or pre-sulfided $NiMoO_4$-SBA catalysts.

The influence of temperature, pressure, residence time and catalyst loadings were investigated. The effect of temperature (330 and 400 °C) on the product yield was investigated in experiments KES_1 (330 °C, 50 bar H_2, 5 % catalyst, 5 h) and KES_2 (400 °C, 50 bar H_2, 5 % catalyst, 5 h) using Kraft lignin. Higher temperature led to a slight increase in lignin liquefaction yields from 48.7 to 49.7 wt% and a clear decrease in char residue from 40.5 to 30 wt%. We also observed that both the water and gas contents increased to >2.0 wt%, indicating that the removal of oxygen from the biomass starts above 330 °C. Moreover, a longer residence time of the reaction (KES_3 (400 °C, 50 bar H_2, 5 % catalyst, 12 h) led to further suppression of the char yield to 27 wt%, and large increases in lignin oil, water and gas content were observed. Hydrogen consumption was measured for the 5 and 12 h residence times and it increased from 1.5 to 3.9 mmol per g of Kraft lignin, simultaneously as the water yield increased from 2.3 % to 7.9 %, due to a higher degree of deoxygenation being achieved.

At a constant temperature of 400 °C, the pressure was increased from 50 to 80 bar (KES_2: 400 °C, 50 bar H_2, 5 % catalyst, 5 h) versus (KES_4: 400 °C, 80 bar H_2, 5 % catalyst, 5 h). This higher pressure ensured a higher solubility of hydrogen in the oil, which resulted in an increase from 49.7 to 61.5 wt% of the oil yield and thereby a higher availability of hydrogen in the vicinity of the catalyst. As seen in Table 5 (KES_2 vs KES_4), this increases the reaction rate and further decreases the unreacted lignin from 9.0 to 4.7 wt%. Furthermore, higher degrees of deoxygenation are favored by increasing the catalyst loadings from 5 to 10 wt%. Consequently, higher lignin-oil yields of 65.1 and lower char yields of 20.6 wt% were achieved for Kraft lignin (KES_4 vs KES_5) with increased catalyst loading. Similarly, for hydrolysis lignin (compare HSE_7, HSE_8 and HSE_{10}), higher loadings of catalyst resulted in increased oil yield and decreased char formation. This could be explained by that when increasing the loading more active sites are available for the adsorption of lignin and in addition, an enhanced hydrogen spillover from Ni_xS_y could occur, resulting in a promotion of the hydrogenation-dehydration reactions.

A comparison of lignin-oil and char yields for Kraft and hydrolysis lignins is presented in Fig. 7. Under identical operating conditions, hydrolysis lignin results display higher lignin oil formation and lower char yields in comparison to Kraft lignin. One of the reasons is that hydrolysis lignin was obtained from enzyme catalytic conditions, making it more active and free from ash and sulfur contents (Table 4), than the lignin materials obtained from chemical processes [20,50]. Generally, additional central factors may be the different chemical structures and compositions of the lignin-types, and in particular their different S/G ratios [51,52]. Moreover, the hydrolysis lignin consisted of both lignin and cellulose (see Fig. 5) and thereby the hydrolysis lignin contains less lignin per mass, and this could also be a factor for producing less char since it is known that lignin often gives large amount of char.

3.2.3. Stability tests

To investigate the stability of the sulfided $NiMoO_4$-SBA catalyst, three consecutive conversions of hydrolysis lignin were conducted using the recycled catalyst (Table S4). Upon completion of the reaction (HES_{10}), the catalyst used was regenerated by calcining the spent catalyst in air at 500 °C for 5 h to burn off any remaining unseparated char or solids. The recycled catalyst was then used for the next reaction cycles as described in the Reaction experiments section 2.5. Table S4 shows that for the experiments with recycled catalyst the conversion and oil yields are similar during repeated cycles. A catalyst weight loss of 10.6 wt% was observed for the first cycle, which is similar to the 8.5 wt% from the TGA thermogram results (Fig. 2a). The second and third cycles were further performed and resulted in negligible weight losses up to 2.0 wt %. Thus, the spent NiMoS-SBA catalyst was found to have good stability and performance comparable to a duplicated HES_{10} experiment (Table 5).

3.2.4. Gas and lignin oil compositions

The gaseous phase composition was quantified, and the results are given in Table 6. The results show a maximum of 5.6 wt% gas product yield measured at room temperature after the reaction. The dominant gas products were CH_4 (0.1–3 wt% on lignin), and CO_2 (0.1–2.4 wt%), with small quantities of olefins C_2-C_4 (<0.7 wt%). The gas-phase formation may be explained by reactions occurring during lignin hydroconversion, along with gas phase reactions. The olefins are derived from the C—C cleavage of alkyl chains or via dehydration of intermediate small alcohols derived from the cleavage of the β-O-4 ether linkage. The formation of CH_4 can be explained by demethylation, which is favored under our conditions. Another possible pathway for methane formation is the reaction of the released CO_2 and CO with H_2. This was also demonstrated for model compounds such as formic and acetic acid over a Ru/TiO_2 catalyst [53,54]. Moreover, the formation of CO_2 and traces of CO can result from decarboxylation and water gas shift reactions. The decarboxylation of –COOH to form larger amounts of CO_2 product was observed for the catalytic hydroconversion at 400 °C (KES_2), but not at

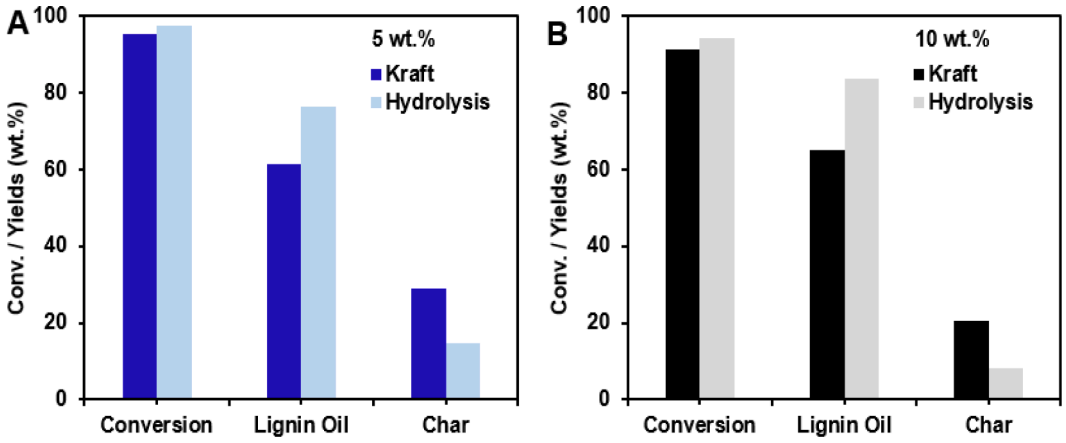

Fig. 7. Comparison of lignin-type, Kraft and hydrolysis, for their conversion, lignin-oil, and char yields (a) 5 wt%; (b) 10 wt% catalyst loading. Conditions: 400 °C, 80 bar H_2, 5 h, and 1200 rpm.

Table 6
The effect of NiMoS-SBA unsupported catalyst on the gas product yield and distributions during lignin hydroconversion. See Table 1 for operating conditions.

Entries	Operating Conditions	Gas Yield (wt.%)	CH_4 (wt.%)	CO_2 (wt.%)	C_{2+} (wt.%)
Kraft Lignin					
KES_0	KL–400–80–5–W_0	0.3	0.1	0.1	0.1
KES_1	KL–330–50–5–W_5	0.1	0.1	0.0	0.0
KES_2	KL–400–50–5–W_5	3.1	1.5	1.1	0.5
KES_3	KL–400–50–12–W_5	5.6	3.0	2.4	0.2
KES_4	KL–400–80–5–W_5	2.4	1.3	1.2	0.2
KES_5	KL–400–80–5–W_{10}	2.1	1.2	0.8	0.1
Hydrolysis Lignin					
HES_6	HL–400–80–5–W_0	0.7	0.3	0.2	0.2
HES_7	HL–400–80–5–W_5	3.1	1.7	1.1	0.5
HES_8	HL–400–80–5–W_{10}	1.2	0.4	0.7	0.1
HES_9	HL–400–80–12–W_{10}	2.6	1.1	0.8	0.7
HES_{10}	HL–400–80–5–W_{20}	1.0	0.3	0.5	0.2

330 °C (KES_1). These results are consistent with those reported previously, suggesting that decarboxylation of carboxylic acids occur at a temperature higher than 350 °C [52,55].

When increasing the temperature (KES_1 versus KES_2) and residence time (KES_2 versus KES_3) for Kraft lignin over the NiMoS-SBA catalyst, the yields of CH_4 and CO_2 increased, whereas it was similar when increasing the pressure (KES_2 versus KES_4). With increasing catalyst content from 5 wt% (KES_4) to 10 wt% (KES_5), the yields of CH_4 and CO_2 were similar. However, a significant decrease in gas yield was observed for hydrolysis lignin while increasing the catalyst loadings from 5, 10 and up to 20 wt% (HES_7, HES_8, and HES_{10}). In contrast to our results, Chowdari *et al.* [56] found that the total yield of gases slightly increased when increasing the catalyst loading for a 20NiMoP/AC from 5 wt% to 10 wt%, respectively from 8.6 to 9.4 % at 400 °C [56]. This can be due to several differences, such as much higher selectivity for the decarboxylation and demethylation with their supported 20NiMoP/AC catalyst and the conditions under which it was used.

The oxygen and hydrogen contents in the lignin-oils are displayed in the form of Van Krevelen diagrams (Fig. 8). The hydrolysis lignin used in this study has a relatively high O/C ratio of 0.51, while that of Kraft lignin is considerably lower, 0.39. This is likely due to differences in the extraction methods, feedstock origins and their different compositions (e.g. cellulose in hydrolysis lignin). Based on the van Krevelen diagrams, the lignin oils show significantly lower O/C ratios (0.02–0.11) and an increase in H/C ratios (1.97–2.26), suggesting that the hydroconversion reactions have occurred to a large extent. It is interesting to note that the estimated Higher Heating Values (HHV) (Tables S1 and S2) are high and similar to those of traditional petroleum-based fuels [57]. Despite the higher starting O/C ratio, hydrolysis lignin showed overall lower oxygen contents in the oils, which possibly can allow easier conversion into high-quality fuels compared to the oil from Kraft lignin. Also, the presence of hydrogen and catalyst resulted in a reduction in sulfur content in the lignin-oils (<0.02 wt%), showing the efficiency of the catalyst for

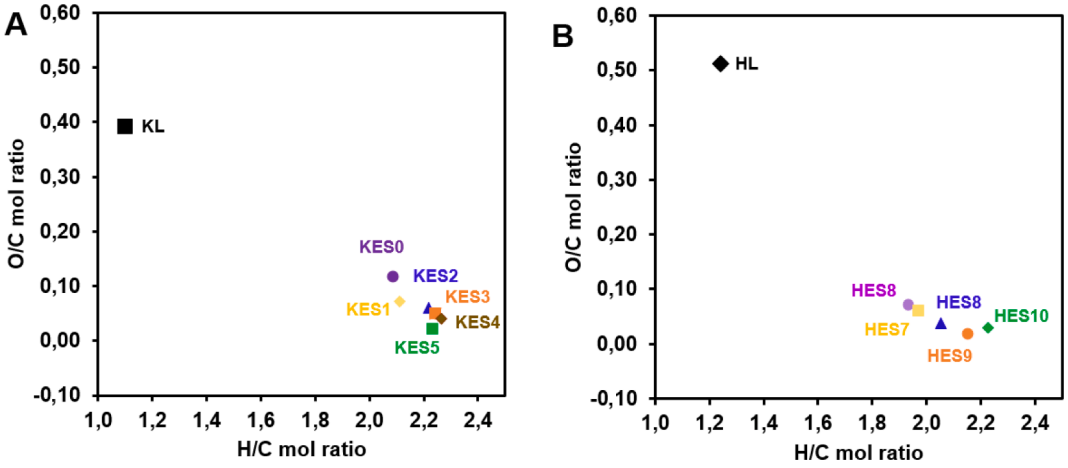

Fig. 8. Van Krevelen diagram of lignin-oils for Kraft and hydrolysis lignins. See Table 1 for operating conditions.

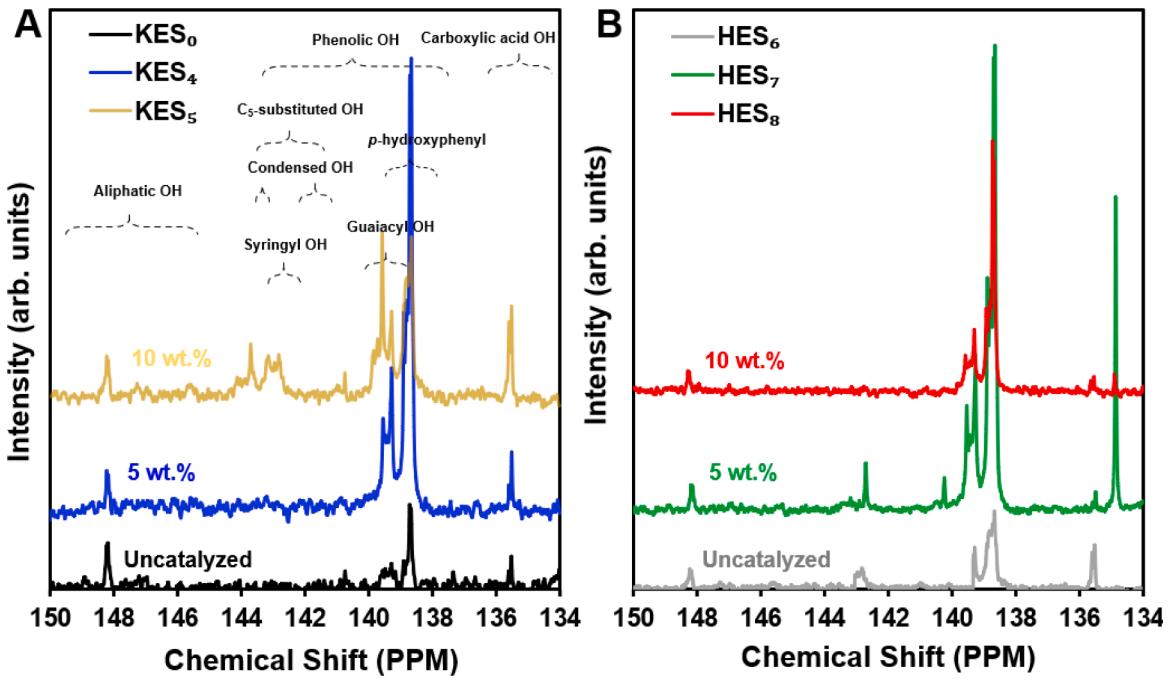

Fig. 9. 31P NMR spectrums of lignin-oil of uncatalyzed, and 5 and 10 wt% of catalyst loading from (a) Kraft and (b) hydrolysis lignins. Conditions: 400 °C, 80 bar, 1200 rpm for 5 h.

HDS reactions (see Tables S1 and S2). In the absence of catalyst (KES_0 and HES_6), the values of oxygen were higher (8.3–11.6 wt%) than for all experiments with unsupported NiMoS-SBA catalyst (1.9–6.3 wt%), which clearly demonstrates the beneficial effect of the catalyst. The above results suggest that NiMoS-SBA is an effective catalyst for hydrogenation, deoxygenation and desulfurization of lignin under the selected conditions. At high temperature and pressure (KES_4), the H/C ratio increases, and it can further increase with extended reaction time as was evident for KES_3 versus KES_2. For reactions performed at 400 °C and 80 bar, an increase in catalyst loading (KES_5 versus KES_4) leads to a decrease in the O/C ratio, which results in that >87 % of the oxygen was removed, compared with the initial feedstocks used.

^{31}P NMR analysis on the lignin-oils was performed to help elucidate the changes that occurred during the reaction. This offers the unique ability to distinguish hydroxyl groups attached to *p*-hydroxyphenyl, guaiacyl, and syringyl units. Fig. 9 shows ^{31}P NMR spectrums of lignin oils obtained under the selected conditions. A compressed compilation of hydroxyl groups in lignin oils and their typical chemical integration ranges are summarized in Fig. 9 along with the quantitative data (Table 7) clearly shows that Kraft and hydrolysis lignin oils were rich in *p*-hydroxyphenyl and guaiacyl OH groups, while syringyl and condensed OH groups (C_5-substituted OH) were observed in small amounts for the highly catalyzed Kraft lignin (10 wt% loaded, KES_5) and less catalyzed (5 wt% loaded, HES_7) and uncatalyzed hydrolysis lignin (HES_6 and HES_7). Small amounts of carboxylic acid (133.6–136 ppm) and aliphatic OH (145–150 ppm) can be distinguished for Kraft and hydrolysis lignin oils as well.

Table 7
The effect of NiMoS-SBA unsupported catalyst on the lignin-oil distribution during lignin hydroconversion.

Structure δ (ppm)	Operating Conditions	Aliphatic OH (mmol/g) 145.4–150.0	Phenolic OH (mmol/g) 137.6–144.0	Carboxylic acid (mmol/g) 133.6–136.0
Kraft Lignin				
KES_0	KL–400–80–5–W_0	0.004	0.080	0.001
KES_1	KL–330–50–5–W_5	0.006	0.170	0.004
KES_2	KL–400–50–5–W_5	0.010	0.270	0.040
KES_3	KL–400–50–12–W_5	0.040	0.420	0.004
KES_4	KL–400–80–5–W_5	0.090	0.300	0.001
KES_5	KL–400–80–5–W_{10}	0.170	0.110	0.010
Hydrolysis Lignin				
HES_6	HL–400–80–5–W_0	0.040	0.590	0.040
HES_7	HL–400–80–5–W_5	0.080	1.170	0.130
HES_8	HL–400–80–5–W_{10}	0.050	0.820	0.020
HES_9	HL–400–80–12–W_{10}	0.040	0.700	0.004
HES_{10}	HL–400–80–5–W_{20}	0.100	0.130	0.014

The total quantity of monomer in the lignin-oils is of high interest to indicate the effect of the unsupported catalyst and various operating conditions on the target product classes in this study. Therefore, all lignin-oils were subjected to GCxGC analysis, with a correction for the hexadecane solvent contribution (Fig. 10). The lignin-oil phase product comprises a complex mixture of monomeric compounds. The monomer composition detected by GCxGC is quite similar for both lignins when other variables are kept constant (listed in Fig. 10). For noncatalyzed reactions shown in the ^{13}P NMR spectrum, the total OH content (Fig. 9, uncatalyzed) in the lignin-oils was lower and dominated by *p*-hydroxyphenyl (phenolic OH groups). This implies that hydrogenolytic cleavage of aryl-O-aryl and aryl-O-aliphatic linkages in the lignin only partially occurred. A series of operating conditions were examined with the presence of the unsupported NiMoS-SBA catalyst and exhibited an important impact on lignin depolymerization, namely enhanced cleavage of C—O—C linkages between lignin units. ^{13}P NMR spectrums showed the presence of a larger amount of *p*-hydroxyphenyl and guaiacyl in the area 138–140 ppm (Fig. 9, catalyzed). By increasing the temperature to 400 °C for Kraft lignin, the methoxyphenol were converted to alkylphenolics by O-demethylation reactions, as confirmed by the GCxGC analysis (KES_1 to KES_2, Fig. 10). This suggests that most of the O-demethylation (–OCH_3) and hence higher CH_4, CO_2 and water yields (Table 5 and Table 6) resulted from cleavage of guaiacol, syringyl and C_5-substituted OH groups occurring at the higher temperature.

By increasing the residence time (KES_2 to KES_3), both alkylated phenolic and aliphatic OH were increased for Kraft lignin (Table 7 and Fig. 10), whereas the carboxylic acid (COOH) was significantly suppressed, leading to the enhancement of CO_2 formation (Table 6). This is

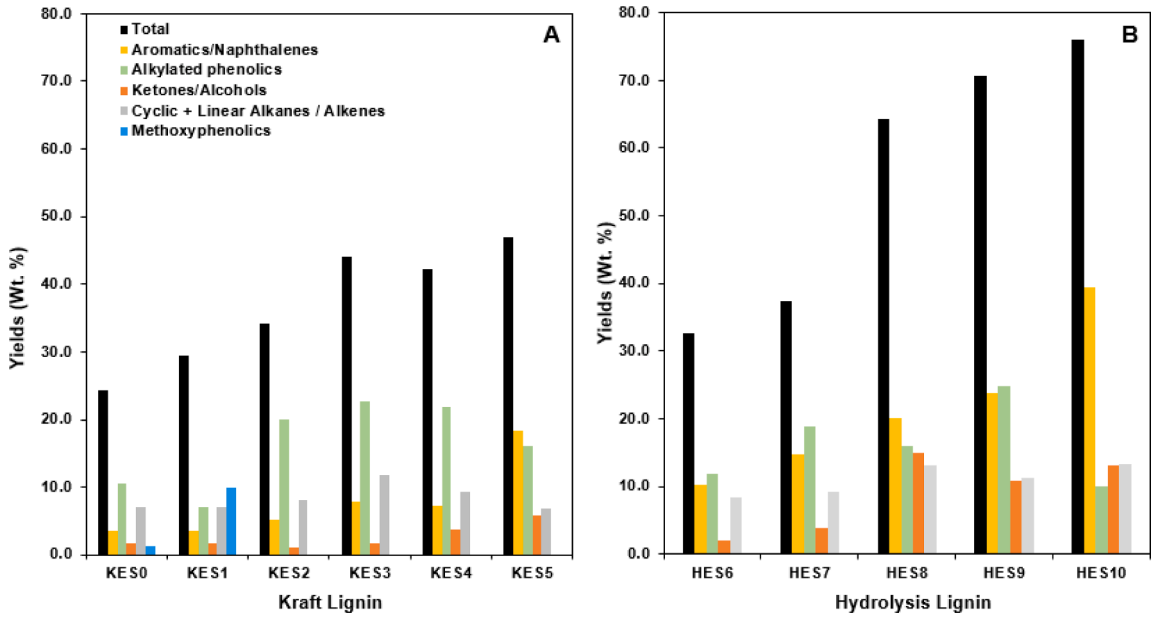

Fig. 10. Monomer evolution according to the operational conditions extracted from GCxGC analysis.

probably due to the reduction of the carboxylic acids accompanied by an increase in solubility of the Kraft lignin in the fluid phase [58]. A similar effect on content of carboxylic acid was observed for hydrolysis lignin while increasing the residence time from 5 to 12 h at 400 °C (HES_8 to HES_9), however; this resulted in slightly decreased phenolic and aliphatic OH contents according to NMR results (Table 7). It is noteworthy to mention that part of the phenolic OH detected by ^{31}P NMR includes those in oligomeric compounds which are not detected by GCxGC analysis. Thus, the enhancement of alkylphenolic and aromatic compounds when increasing the residence time from 5 h to 12 h, as shown in the GCxGC results (HES_8 to HES_9, Fig. 10), can be explained by a deep cleavage of the oligomeric compounds (Table 7). As can be seen in Fig. 9, the C5-substituted OH units for uncatalyzed (0 wt%, KES_0) and less catalyzed Kraft lignin (5 wt%, KES_4) were not observed, whereas it was observed for the highly catalyzed Kraft lignin (10 wt%, KES_5). For hydrolysis lignin, the uncatalyzed (0 wt%, HES_6) and less catalyzed (5 wt%, HES_7) lignin showed small amounts of C5-substituted OH units, however; none were observed at the higher catalyst loading (10 wt% HES_8). Although the reaction conditions were nearly identical, the depolymerization and cleavage of C—O bonds differed to a certain extent between the lignins.

Upon increasing the catalyst loading from 10 wt% (HES_8) to 20 wt% (HES_{10}) for hydrolysis lignin, all hydroxylic groups and particularly the phenolic OH content decreased by eightfold (Table 7), which was accompanied by a significant reduction in the char yield and an enhancement in lignin-oil yields (HES_{10}, Table 5). These changes also resulted in an increase in aromatic, and a decrease in alkylated phenolics and aliphatic OH/Ketones yields (HES_{10}, Fig. 10). As shown by comparison between the Kraft and hydrolysis lignins in Fig. 9, the high correlation between alkyl phenolics and aromatics is strongly dependent on the composition and structural complexity of the lignins which influences their hydroconversion reactivity.

The total monomer yield ranged from 25.1 to 47.0 wt% for Kraft lignin (KES_0 to KES_5, Fig. 10) and from 32.7 to 76.0 wt% for hydrolysis lignin (HES_6 to HES_{10}) under the various reaction conditions. Alkylphenolics are the dominant chemical group from Kraft (7.0–22.7 wt%) and hydrolysis (11.9–24.8 wt%) lignin oil, except at higher than 10 wt% of catalyst loading for both the Kraft and hydrolysis lignins in which case the aromatics were the major compound from Kraft (18.3 wt%) and hydrolysis lignin oil (39.4 wt%). However, the proportion of the oil products composed of aromatics/naphthalenes varies between the lignin oils, where higher aromatic yields of 14.7 wt% were obtained for hydrolysis lignin (HES_7) compared to 7.3 wt% for Kraft lignin oil (KES_4) at the same operating conditions. When comparing the 10 wt% loading of catalyst at the same conditions (HES_8 vs KES_5), it is apparent that hydrolysis lignin produces higher lignin-oil yields of 83.7 wt% compared to Kraft lignin-oil of 65.1 wt% (Table 5), corresponding to 64.3 and 47.0 wt% of monomer yields respectively (Fig. 10). This has been previously confirmed using model compounds over NiS_2/MoS_2 [50]. It was reported that only an appropriate proportion of donor phase (NiS_2) to acceptor phase (MoS_2) could produce the maximum HDO activity. More specifically, the hydrogenation activity was enhanced in the presence of NiS_2, leading to an increase in cyclohexane derivative selectivity and deoxygenation degree. The authors claimed that an optimal Ni/(Ni + Mo) molar ratio of 0.3 was important to achieve the highest activity with 99.8 % deoxygenation degree [50]. In our study, this ratio, determined from XPS analysis, was about 0.33, which is in good agreement with the reported optimum.

In a recent study, Chowdari *et al.* [56] reported a total monomer yield of 45.7 wt% over 10 wt% bimetallic 20NiMoP/AC for Kraft lignin at 400 °C and 100 bar with no added solvents. These findings are in line with our results for Kraft lignin, with monomer yields in the range of 42.3–47.0 wt%. However, the aromatics were reported to be lower (8.7 wt%) for the 20NiMoP/AC catalyst in comparison to the unsupported NiMoS-SBA (18.3 wt%), whereas opposite levels in the yields of alkylphenolics resulted (25.0 wt% for 20NiMoP/AC and l6.1 wt% for NiMoS-SBA). A higher solid yield was obtained for our operating conditions, but notably at lower pressures of 50–80 bar. The adjustment of pressure, residence time (from 5 to 12 h) and catalyst loadings can likely further reduce the char formation and significantly increase lignin-oil and monomeric yields. Interestingly by increasing the catalyst loading from 5 % to 10 % (KES_4 to KES_5), the degree of deoxygenation is strongly increased from about 46.0 to 60.5 % and therefore resulted in an increment of aromatics from 7.3 to 18.3 wt% respectively for Kraft lignin oil. This was also evident by a reduction of the calculated oxygen content of the oils (Tables S2 and S3) and indicating that the unsupported catalyst exhibits better selectivity for deoxygenated products under nearly identical conditions.

In the case of hydrolysis lignin, the effect of catalyst loading (from 5 to 20 wt%) on lignin oil yields and composition was investigated at 400 °C using the same unsupported NiMoS-SBA catalyst. By increasing the catalyst loading from 5 to 10 wt%, the monomer yield was

significantly enhanced from 46.6 to 64.3 wt% with a suppression of char to 8.3 wt% (HES_8). While increasing the residence time (from 5 to 12 h), the monomer yield was further enhanced from 64.3 to 70.6 wt% with a suppression of char from 8.3 down to 3.9 wt% for HES_8 and HES_9 respectively. Upon increasing the catalyst loading to 20 wt%., the total monomer yield was still further increased to 76.0 wt%. The char formation was suppressed considerably at the highest catalyst loading from 8.3 to 4.6 wt% (HES_{10}) due to the depolymerization reactions involving the bimetallic NiMoS-SBA catalyst. These results are also in agreement with data reported by Chowdari *et al.* [56], suggesting that the repolymerization reactions leading to char are likely thermal and not catalytic, while the depolymerization reactions are catalytic. However, Chowdari *et al.* found that higher temperature (>400 °C) leads to the formation of more char and less oil yield [56]. In our study, the main objective was to explore reaction conditions that are favorable using an unsupported NiMoS-SBA catalyst. The results obtained at 20 wt% loading of catalyst for hydrolysis lignin showed that over 87 wt% of lignin can be depolymerized, which consists of 39 wt% of aromatics/naphthalenes with the lowest alkylphenolic yield of 10.1 wt%.

Like a previously published work [59], TGA analysis was used to evaluate the volatility of lignin-oils resulting from biomass conversion. Comparison of the volatilities of Kraft (KES_5) and hydrolysis (HES_8) lignin-oils were performed with oils produced under the same operating conditions (400 °C, 80 bar, 5 h). Fig. 11 shows that a complete weight loss for both lignin-oils was observed when increasing the temperature to 500 °C under N_2 flow. The hydrolysis lignin oil contains less thermally stable compounds, as indicated by its higher volatilization rate at 200 °C. In addition, it requires more energy (higher temperature) to completely volatilize the produced Kraft lignin-oil (>300 °C). This difference may be due to the influence of the origin of the lignins and their extraction processes. More importantly, both lignin-oils followed the TGA curve of diesel oil, particularly for hydrolysis lignin-oil [59]. This implies that the hydrolysis lignin-oil contains a higher share of low boiling point compounds than the Kraft lignin-oil.

3.2.5. Reaction mechanisms

Based on the above analysis and discussion, lignin hydroconversion to produce lignin-oils, gas and residual solids involves various reaction pathways depending on the lignin composition, and operating conditions. Numerous studies have proposed and summarized schemes for the conversion of Kraft lignin by depolymerization [56,60–63]. In contrast

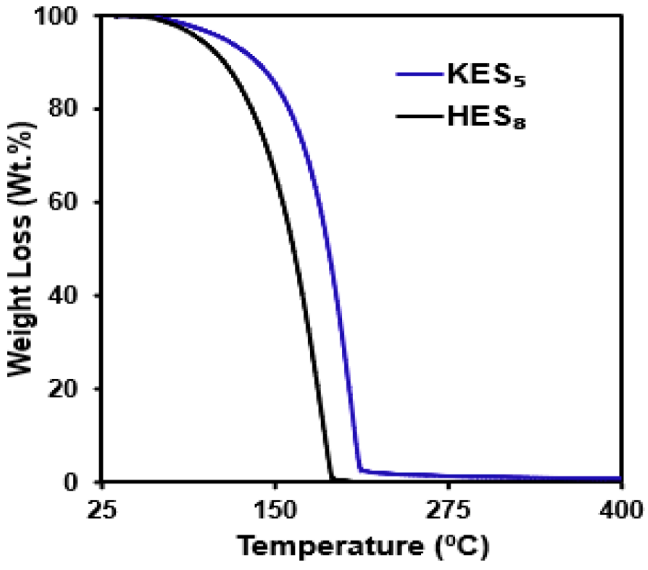

Fig. 11. Weight loss curves of lignin-oils obtained at 400 °C, 80 bar and 10 wt % catalyst to Kraft (KES5) and hydrolysis (HES8) lignin. See Table 1 for operating conditions.

to Kraft lignin, limited studies have investigated reaction pathways of the depolymerization of enzymatic hydrolysis lignin. Chudakov *et al.* and Pikovskoi *et al.* [64,65] proposed a unique macrostructural composition of hydrolysis lignin consisting of about 7000 peaks of deprotonated molecules $[M—H]^-$. The largest detected molecules were decamers with molecular weights up to 1600 Da, containing up to 10 aromatic units with an average molecular weight of 150 Da per structural unit [64,65]. Pikovskoi *et al.* also claimed that depolymerization of hydrolysis lignin released coniferous lignin corresponding to the abundant guaiacyl structural unit of about 196 Da. In addition to Chudakov and Pikovskoi suggestions, the hydrolysis lignin in this work showed the presence of cellulosic units by means of solid-state ^{13}C NMR (Fig. 5), as depicted in Scheme 1.

According to the reported data in Table 5, Table 6 and Fig. 10 the non-catalytic experiments favored the formation of solid-char. We suggest that the highly reactive intermediates (oxygenated compounds) formed during the thermal decomposition of lignin results in condensation (Scheme 1A) and large char formation. Generally, the alkylation reactions predominantly have a significant role to restrain the condensation reaction by multiple substitutions of the abundantly formed positively charged species (e.g., $R—^+O—CH_3$) with electron-rich active species (negatively charged Aryl, $Ar^-—O—R$) that jointly affect the electron distribution of both lignins [67,68]. Without the presence of catalyst (Scheme 1A), a negatively charged aromatic, ring rich in electrons, is mostly formed ($Ar^-—O—R$) and subjected to substitution of phenol-ether and/or alkylphenolic ($Ar—R—^+OH$ and $Ar—^+O—R$). In addition to the resonance effect, the inductive effect of the positively charged moieties ($R—^+O—R$) leads to higher electron densities, which are involved in lignin condensation by forming benzylic carbocations and thereby enhance char formation [67,68]. This suggestion is supported by the fact that the formed alcohols/ketones, olefins and CH_4 were present in the lowest amounts and only account respectively for less than 0.2 and 0.3 wt% of products for both lignins during uncatalyzed reactions (KES_0 and HES_6).

In the presence of the unsupported NiMoS-SBA catalyst (Scheme 1B–E), the hydrotreatment of both lignins becomes relevant and contributes to heterogeneous catalyzed processes at higher temperatures. Due to the difference in structural and chemical composition of hydrolysis lignin, a higher yield of small ketone and aliphatic alcohols in hydrolysis lignin-oils (13.2 wt%) were obtained due to the depolymerization and ring opening of cellulose and furan units present in hydrolysis lignin, as was evident from the ^{13}C NMR spectrum and GCxGC results (Fig. 5 and Fig. 10). According to Shuai and Saha [69] alcohols, ketones and aldehydes can block the electron-rich sites on the aromatic ring and the benzylic cation on the side chain, which would reduce the lignin condensation. The larger amount of alcohols and ketones formed in hydrolysis lignin (Fig. 9) could be one reason for the lower char amount and enhanced monomeric yields in the liquid phase (Scheme 1B). Huang et al. [68] examined lignin depolymerization in the presence of ethanol and suggested that the C-alkylation and O-alkylation reactions are important reactions for decreasing the condensation and thereby the char formation. We therefore suggest that during the depolymerization of hydrolysis lignin, higher stability of the aromatics (negatively charged moieties) via C- and O-alkylation reactions mainly come from cleaved and dehydration of the aliphatic OH and ketones. Additionally, these small ketones/alcohols derived from lignin can be hydroconverted to small alkenes via cracking dehydration (Scheme 1C). The primary stable monomers obtained from lignin (Scheme 1D) may undergo secondary hydrogenation reactions of oxygenates to form more stable monomer products (Scheme 1E).

Generality across different mechanisms can be accepted considering the complexity of the types of lignin depolymerized and may play a role in the identification of effective catalysts. In this study, evidence suggests that a combination of mechanisms hinders the formation of oligomeric C—C linkages and thus blocks the re-condensation reactions. From our set of experiments and the literature [6,66–68], Scheme 2

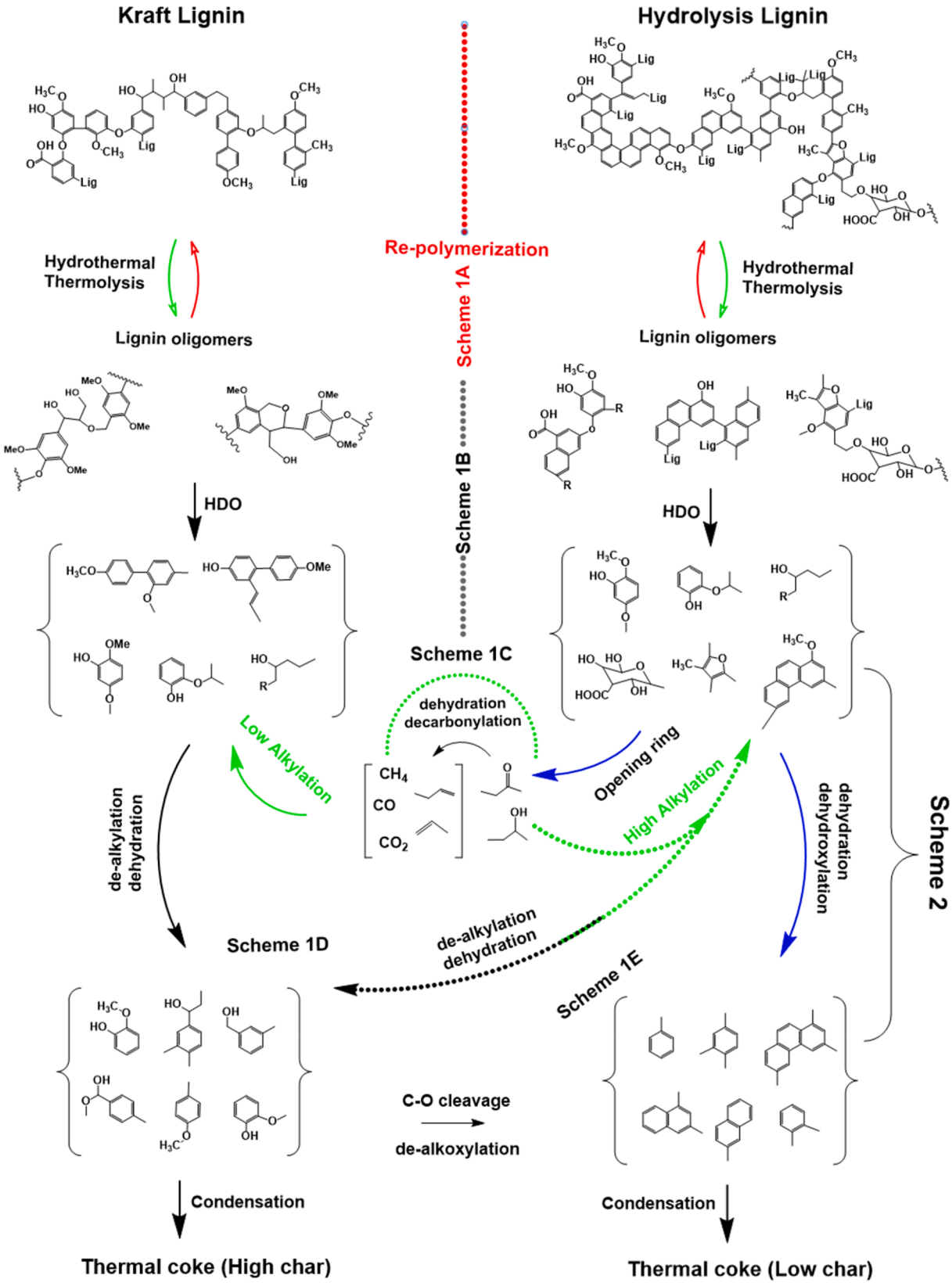

Scheme 1. Proposed pathways in non-catalytic and catalytic polymerization of Kraft and hydrolysis lignins.

summarizes the most important aspects hindering the repolymerization over the unsupported NiMoS-SBA catalyst. We suggest that the condensation reaction rate was slowed down by blockage of the electron-rich sites (aromatic ring) via hydrogen spillover generated on Ni_xS_y, which prevented the formation of benzylic cations. Thereafter, the negatively charged aryl molecules either undergo hydrogenolysis interactions in series or in parallel reactions with the supplied hydrogen (H^+) and/or with alkylated species present in the lignin-oils. These

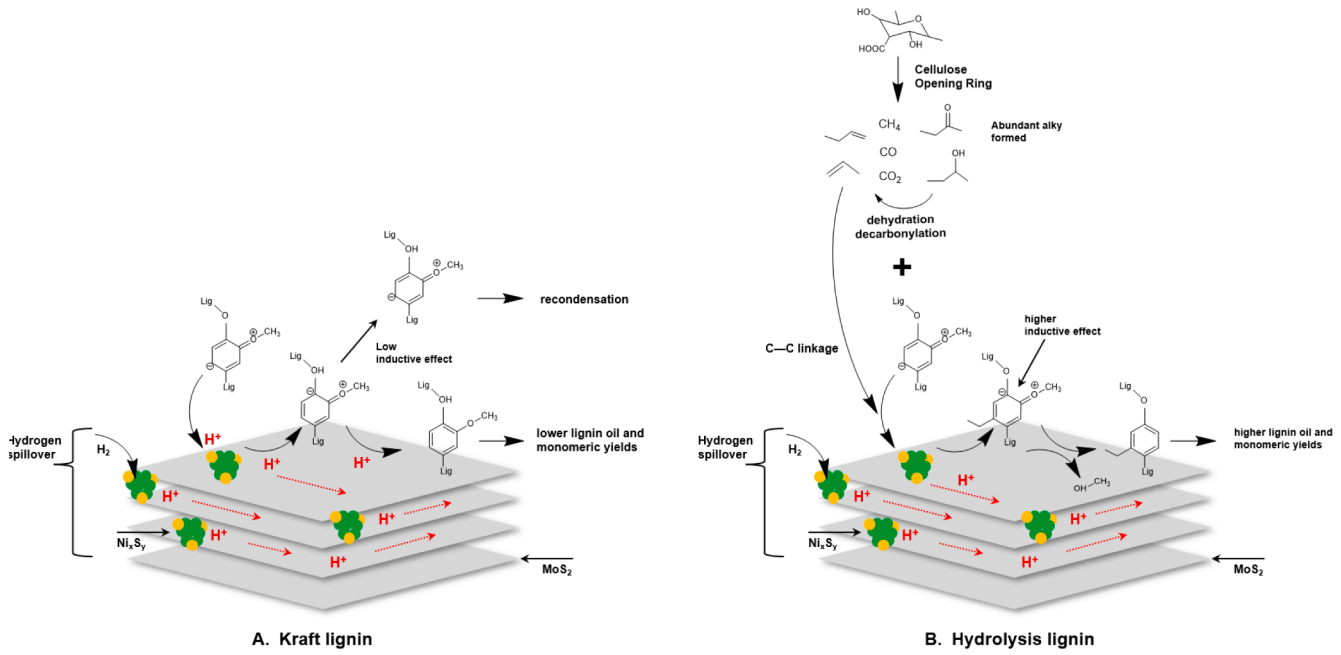

Scheme 2. Proposed reaction mechanism for stabilizing benzylic carbocations from hydrolysis and Kraft lignins over NiMoS catalysts.

alkylated species are present in greater quantities from hydrolysis lignin (13.2 wt%) and thus serve as promoters for depolymerization compared to the lower quantities of alkylated species from Kraft lignin (6.8 wt%).

We also suggest that the stabilization of aromatic rings is enhanced by a combination of interunit C(aryl)—C(alkyl) linkages and the supplied hydrogen species as shown for hydrolysis lignin (Scheme 2B), whereas these factors are less dominant in the case of Kraft lignin (Scheme 2A). This accounts for the higher resulting monomeric yields and lower char formation from hydrolysis lignin compared to Kraft lignin. In this study, our hypothesis is built on the importance of the inductive effect that provides higher electron densities on methoxy groups (R—$^{+}$O—CH_3) due to the formation of interunit C(aryl)—C(alkyl) linkages, which create higher electron densities on the aromatic ring to further stabilize it and block the reactive benzylic positions.

Based on literature, our proposal agrees with that of by Shuai *et al.* [6,69] that found that formaldehyde acted as a lignin stabilizer by blocking the reactive benzylic positions of intermediates [6]. Also in agreement with our results, Huang et *al.* [68] suggested that ethanol is a capping agent acting as a scavenger for formaldehyde formed by removal of methoxy groups from the lignin, that thereby suppresses repolymerization reactions involving formaldehyde [68].

To summarize, lignin valorization is more efficient with hydrolysis lignin compared to Kraft lignin, which could be seen by a significantly higher amount of monomer bio-oil produced and lower char formation. This is be explained by (i) differences in the structure of hydrolysis lignin, which facilitates thermal decomposition, (ii) less lignin per mass unit in hydrolysis lignin, due to the presence of cellulose (iii) less inorganic ash in the hydrolysis lignin which could negatively affect the catalytic reactions and (iv) suppressing the repolymerization by reactions with components formed from the cellulose.

4. Conclusions

In this study, we have for the first time according to our knowledge compared the reductive catalytic lignin depolymerization using Kraft and hydrolysis lignin and we found large differences. We have synthesized a highly active unsupported NiMoS catalyst that was used in this work. The use of the unsupported NiMoS-SBA demonstrated a potentially promising approach to obtain bio-oils with a high proportion of aromatic and alkylphenolic compounds. The influence of the operating conditions (temperatures, pressure and time) with various catalyst loadings of 5–20 wt%, were evaluated in terms of product yields and composition.

Catalytic hydrotreatment experiments with hydrolysis lignin exhibited deeper deoxygenation performance in comparison to Kraft lignin. The increase in the reaction temperature, between 330 and 400 °C, dramatically enhanced the cleavage of C—O—C bonds, especially increasing alkylated phenolics from 7.0 to 20.1 wt% yield respectively. On the other hand, it was observed that as the pressure increased from 50 to 80 bar and residence time increased, the yields in oil and monomeric compounds also increased, and char formation could be suppressed to a certain extent. Interestingly, the monomers yield was the highest and the char was the lowest for hydrolysis lignin at comparable reaction conditions. In addition, the NMR and GCxGC analysis demonstrated that with an increase in catalyst loading, the phenolic OH groups were decreased in the product oil which resulted in an increment in the aromatics yield. Comparing the volatilities, lignin-oils from Kraft and hydrolysis lignin showed a complete volatilization which indicates a high content of low boiling compounds, particularly for hydrolysis lignin-oil.

The unsupported NiMoS catalyst displayed notable deoxygenation activity, with 87 wt% lignin-oil yield from hydrolysis lignin, with less than 5 wt% char yield. Remarkably the significant reduction of char from hydrolysis lignin compared to Kraft lignin led to an increase in water and lignin-oil yields, resulting in higher selectivity and yield of aromatics. These results highlighted the importance of the chemical stability and the nature of processed lignins that arise directly from the oligomer composition of the lignin, and their correlation between depolymerization yields and the ratio of C—O—C and C—C linkages in the lignins. From the experimental results, the higher monomeric yield from hydrolysis lignin can be explained by that the hydrolysis lignin more easily depolymerizes. Moreover, the hydrolysis lignin also contains less lignin (since it contains both lignin and cellulose) and less ash, which also are important reasons for the lower char production and higher bio-oil yield when using hydrolysis lignin. In addition, the molecular binding mechanism of hydrolysis lignin is a key to generate higher-value small molecules through depolymerization. Results suggested that the high electron densities of the formed small molecules from cellulose decomposition could interact with the aromatic ring and influence the reactivity of the benzylic carbocations formation. Apart

from effective hydrotreating cleavage, the catalyst demonstrates a good activity and stability over multiple regeneration cycles; however, long testing will be required in a pilot scale reactor to assess its total lifetime in the future.

Declaration of Competing Interest

The authors declare that they have no known competing financial interests or personal relationships that could have appeared to influence the work reported in this paper.

Data availability

Data will be made available on request.

Acknowledgements

We would like to acknowledge the collaboration with Preem, Borealis and RISE in this project. We would like to thank Sekab for kindly providing us the hydrolysis lignin. We would like to acknowledge Vinnova (Vinnväxt) and Swedish Energy Agency (P47511-1) for the funding. We would like to thank the Swedish NMR Centre for the access to NMR facilitates and Chalmers Material Characterization Laboratory (CMAL) for CHONS, XRD, XPS, SEM and TEM access/measurements.

Appendix A. Supplementary data

Supplementary data to this article can be found online at https://doi.org/10.1016/j.cej.2022.139829.

References

[1] A. Shrotri, H. Kobayashi, A. Fukuoka, Chapter Two – Catalytic Conversion of Structural Carbohydrates and Lignin to Chemicals, Adv. Catal. 60 (2017) 59–123, https://doi.org/10.1016/bs.acat.2017.09.002.
[2] L.B. Davin, M. Jourdes, A.M. Patten, K.-W. Kim, D.G. Vassão, N.G. Lewis, Dissection of lignin macromolecular configuration and assembly: Comparison to related biochemical processes in allyl/propenyl phenol and lignan biosynthesis, Nat. Prod. Rep. 25 (2008) 1015–1090, https://doi.org/10.1039/B510386J.
[3] G.J.M. van der KERK, Organotin Chemistry: Past, Present, and Future, in: Organotin Compd. New Chem. Appl., 1976: 1–25. doi: 10.1021/ba-1976-0157.ch001.
[4] E.M. Anderson, M.L. Stone, R. Katahira, M. Reed, W. Muchero, K.J. Ramirez, G. T. Beckham, Y. Román-Leshkov, Differences in S/G ratio in natural poplar variants do not predict catalytic depolymerization monomer yields, Nat. Commun. 10 (2019) 2033, https://doi.org/10.1038/s41467-019-09986-1.
[5] T. Renders, G. Van den Bossche, T. Vangeel, K. Van Aelst, B. Sels, Reductive catalytic fractionation: state of the art of the lignin-first biorefinery, Curr. Opin. Biotechnol. 56 (2019) 193–201, https://doi.org/10.1016/j.copbio.2018.12.005.
[6] L. Shuai, M.T. Amiri, Y.M. Questell-Santiago, F. Héroguel, Y. Li, H. Kim, R. Meilan, C. Chapple, J. Ralph, J.S. Luterbacher, Formaldehyde stabilization facilitates lignin monomer production during biomass depolymerization, Science 80 (354) (2016) 329–333, https://doi.org/10.1126/science.aaf7810.
[7] D.S. Bajwa, G. Pourhashem, A.H. Ullah, S.G. Bajwa, A concise review of current lignin production, applications, products and their environmental impact, Ind. Crops Prod. 139 (2019), 111526, https://doi.org/10.1016/j.indcrop.2019.111526.
[8] K. Olofsson, M. Bertilsson, G. Lidén, A short review on SSF – an interesting process option for ethanol production from lignocellulosic feedstocks, Biotechnol. Biofuels. 1 (2008) 7, https://doi.org/10.1186/1754-6834-1-7.
[9] J.A. Toledo-Antonio, M.A. Cortés-Jácome, C. Angeles-Chávez, J. Escobar, M. C. Barrera, E. López-Salinas, Highly active CoMoS phase on titania nanotubes as new hydrodesulfurization catalysts, Appl. Catal. B Environ. 90 (1) (2009) 213, https://doi.org/10.1016/j.apcatb.2009.03.024.
[10] M. Dan, J. Xiang, F. Wu, S. Yu, Q. Cai, L. Ye, Y. Ye, Y. Zhou, Rich active-edge-site MoS2 anchored on reduction sites in metal sulfide heterostructure: Toward robust visible light photocatalytic hydrogen sulphide splitting, Appl. Catal. B Environ. 256 (2019), 117870, https://doi.org/10.1016/j.apcatb.2019.117870.
[11] R. Jastrzebski, Catalytic C-C Bond Cleavage for the Production of Chemicals from Lignin, Universiteit Utrecht, Netherlands, 2016 https://dspace.library.uu.nl/handle/1874/328466.
[12] K. Liu, Catalytic Hydrodeoxygenation of Bio-oil and Model Compounds, Imperial College London London, UK, 2015.
[13] J.P.W. Inwood, L. Pakzad, P. Fatehi, Production of Sulfur Containing Kraft Lignin Products, Bioresources. 13 (2017) 53–70.
[14] C.R. Kumar, N. Anand, A. Kloekhorst, C. Cannilla, G. Bonura, F. Frusteri, K. Barta, H.J. Heeres, Solvent free depolymerization of Kraft lignin to alkyl-phenolics using supported NiMo and CoMo catalysts, Green Chem. 17 (2015) 4921–4930, https://doi.org/10.1039/C5GC01641J.
[15] M. Tymchyshyn, A. Rezayan, Z. Yuan, Y. Zhang, C., (Charles) Xu, Reductive hydroprocessing of hydrolysis lignin over efficient bimetallic catalyst MoRu/AC, Ind. Eng. Chem. Res. 59 (2020) 17239, https://doi.org/10.1021/acs.iecr.0c01151.
[16] S. Wang, W. Gao, L.-P. Xiao, J. Shi, R.-C. Sun, G. Song, Hydrogenolysis of biorefinery corncob lignin into aromatic phenols over activated carbon-supported nickel, Sustain, Energy Fuels. 3 (2019) 401–408, https://doi.org/10.1039/C8SE00359A.
[17] Y. Bai, K. Cui, Y. Sang, K. Wu, F. Yan, F. Mai, Z. Ma, Z. Wen, H. Chen, M. Chen, Y. Li, Catalytic Depolymerization of a Lignin-Rich Corncob Residue into Aromatics in Supercritical Ethanol over an Alumina-Supported NiMo Alloy Catalyst, Energy & Fuels. 33 (2019) 8657–8665, https://doi.org/10.1021/acs.energyfuels.9b01457.
[18] J. Horáček, F. Homola, I. Kubičková, D. Kubička, Lignin to liquids over sulfided catalysts, Catal. Today. 179 (2012) 191–198, https://doi.org/10.1016/j.cattod.2011.06.031.
[19] Y. Sang, M. Chen, F. Yan, K. Wu, Y. Bai, Q. Liu, H. Chen, Y. Li, Catalytic Depolymerization of Enzymatic Hydrolysis Lignin into Monomers over an Unsupported Nickel Catalyst in Supercritical Ethanol, Ind. Eng. Chem. Res. 59 (2020) 7466–7474, https://doi.org/10.1021/acs.iecr.0c00812.
[20] Q. Liu, Y. Bai, H. Chen, M. Chen, Y. Sang, K. Wu, Z. Ma, Y. Ma, Y. Li, Catalytic conversion of enzymatic hydrolysis lignin into cycloalkanes over a gamma-alumina supported nickel molybdenum alloy catalyst, Bioresour. Technol. 323 (2021), 124634, https://doi.org/10.1016/j.biortech.2020.124634.
[21] J.L. Braun, K.M. Holtman, J.F. Kadla, Lignin-based carbon fibers: Oxidative thermostabilization of kraft lignin, Carbon N. Y. 43 (2005) 385–394, https://doi.org/10.1016/j.carbon.2004.09.027.
[22] G. Jiang, D.J. Nowakowski, A.V. Bridgwater, A systematic study of the kinetics of lignin pyrolysis, Thermochim. Acta. 498 (2010) 61–66, https://doi.org/10.1016/j.tca.2009.10.003.
[23] Y. Xie, D. Kocaefe, C. Chen, Y. Kocaefe, Review of Research on Template Methods in Preparation of Nanomaterials, J. Nanomater. 2016 (2016) 2302595, https://doi.org/10.1155/2016/2302595.
[24] X. Meng, C. Crestini, H. Ben, N. Hao, Y. Pu, A.J. Ragauskas, D.S. Argyropoulos, Determination of hydroxyl groups in biorefinery resources via quantitative 31P NMR spectroscopy, Nat. Protoc. 14 (9) (2019) 2627–2647.
[25] G. Soave, Equilibrium constants from a modified Redlich-Kwong equation of state, Chem. Eng. Sci. 27 (1972) 1197–1203, https://doi.org/10.1016/0009-2509(72)80096-4.
[26] S. Perry, R.H. Perry, D.W. Green, J.O. Maloney, Perry's chemical engineers' handbook (2000), https://doi.org/10.5860/choice.38-0966.
[27] M. Oghbaei, O. Mirzaee, Microwave versus conventional sintering: A review of fundamentals, advantages and applications, J. Alloys Compd. 494 (2010) 175–189, https://doi.org/10.1016/j.jallcom.2010.01.068.
[28] H. Liu, C. Yin, X. Li, Y. Chai, Y. Li, C. Liu, Effect of NiMo phases on the hydrodesulfurization activities of dibenzothiophene, Catal. Today. 282 (2017) 222–229, https://doi.org/10.1016/j.cattod.2016.08.002.
[29] R.A. Madeley, S.E. Wanke, Variation of the dispersion of active phases in commercial nickel-molybdenum/γ-alumina hydrotreating catalysts during oxidative regeneration, Appl. Catal. 39 (1988) 295–314, https://doi.org/10.1016/S0166-9834(00)80956-2.
[30] J.L. Brito, A.L. Barbosa, Effect of phase composition of the oxidic precursor on the HDS activity of the sulfided molybdates of Fe(II), Co(II), and Ni(II), J. Catal. 171 (1997) 467–475, https://doi.org/10.1006/jcat.1997.1796.
[31] B. Moreno, E. Chinarro, M.T. Colomer, J.R. Jurado, Combustion synthesis and electrical behavior of nanometric β-NiMoO4, J. Phys. Chem. C. 114 (2010) 4251–4257, https://doi.org/10.1021/jp907870a.
[32] Y. Tan, K. Yu, T. Yang, Q. Zhang, W. Cong, H. Yin, Z. Zhang, Y. Chen, Z. Zhu, The combinations of hollow MoS2 micro@nano-spheres: one-step synthesis, excellent photocatalytic and humidity sensing properties, J. Mater. Chem. C. 2 (2014) 5422–5430, https://doi.org/10.1039/C4TC00423J.
[33] G. An, L. Chenguang, Y. Hou, X. Zhang, Y. Liu, Transition metal dichalcogenide materials: Solid-state reaction synthesis of nanocrystalline nickel disulfide, Mater. Lett. 62 (2008) 2643–2646, https://doi.org/10.1016/j.matlet.2008.01.005.
[34] N.H. Idris, M.M. Rahman, S.-L. Chou, J.-Z. Wang, D. Wexler, H.-K. Liu, Rapid synthesis of binary α-NiS–β-NiS by microwave autoclave for rechargeable lithium batteries, Electrochim. Acta. 58 (2011) 456–462, https://doi.org/10.1016/j.electacta.2011.09.066.
[35] Z. Hou, C. Shu, J. Long, Honeycomb-like Ni3S2 supported on Ni foam as high performance free-standing cathode for lithium oxygen batteries, Electrochim. Acta. 290 (2018) 657–665, https://doi.org/10.1016/j.electacta.2018.08.139.
[36] R. Karthikeyan, D. Thangaraju, N. Prakash, Y. Hayakawa, Single-step synthesis and catalytic activity of structure-controlled nickel sulfide nanoparticles, CrystEngComm. 17 (2015) 5431–5439, https://doi.org/10.1039/C5CE00742A.
[37] B. Yoosuk, D. Tumnantong, P. Prasassarakich, Amorphous unsupported Ni-Mo sulfide prepared by one step hydrothermal method for phenol hydrodeoxygenation, Fuel. 91 (2012) 246–252, https://doi.org/10.1016/j.fuel.2011.08.001.
[38] B. Pillay, M.R. Mathebula, H.B. Friedrich, The oxidative dehydrogenation of n-hexane over Ni-Mo-O catalysts, Appl. Catal. A Gen. 361 (2009) 57–64, https://doi.org/10.1016/j.apcata.2009.03.032.
[39] K.-K. Liu, W. Zhang, Y.-H. Lee, Y.-C. Lin, M.-T. Chang, C.-Y. Su, C.-S. Chang, H. Li, Y. Shi, H. Zhang, C.-S. Lai, L.-J. Li, Growth of Large-Area and Highly Crystalline MoS2 Thin Layers on Insulating Substrates, Nano Lett. 12 (2012) 1538–1544, https://doi.org/10.1021/nl2043612.

[40] Z. Yang, D. Gao, J. Zhang, Q. Xu, S. Shi, K. Tao, D. Xue, Realization of high Curie temperature ferromagnetism in atomically thin MoS2 and WS2 nanosheets with uniform and flower-like morphology, Nanoscale. 7 (2015) 650–658, https://doi.org/10.1039/C4NR06141A.
[41] Y. Pu, B. Hallac, A.J. Ragauskas, Plant Biomass Characterization: Application of Solution- and Solid-State NMR Spectroscopy, in: Aqueous Pretreat. Plant Biomass Biol. Chem. Convers. to Fuels Chem., 2013. doi: 10.1002/9780470975831.ch18.
[42] S. Laurichesse, L. Avérous, Chemical modification of lignins: Towards biobased polymers, Prog. Polym. Sci. 39 (7) (2014) 1266, https://doi.org/10.1016/j.progpolymsci.2013.11.004.
[43] J.L. Wen, S.L. Sun, B.L. Xue, R.C. Sun, Recent advances in characterization of lignin polymer by solution-state nuclear magnetic resonance (NMR) methodology, Materials (Basel) 6 (1) (2013) 359, https://doi.org/10.3390/ma6010359.
[44] L. Fu, S.A. McCallum, J. Miao, C. Hart, G.J. Tudryn, F. Zhang, R.J. Linhardt, Rapid and accurate determination of the lignin content of lignocellulosic biomass by solid-state NMR, Fuel. 141 (2015) 39, https://doi.org/10.1016/j.fuel.2014.10.039.
[45] A. Berlin, M. Balakshin, N. Gilkes, J. Kadla, V. Maximenko, S. Kubo, J. Saddler, Inhibition of cellulase, xylanase and β-glucosidase activities by softwood lignin preparations, J. Biotechnol. 125 (2) (2006) 198–209.
[46] R. Samuel, M. Foston, N. Jaing, S. Cao, L. Allison, M. Studer, C. Wyman, A. J. Ragauskas, HSQC (heteronuclear single quantum coherence) 13C–1H correlation spectra of whole biomass in perdeuterated pyridinium chloride-DMSO system: An effective tool for evaluating pretreatment, Fuel. 90 (9) (2011) 2836, https://doi.org/10.1016/j.fuel.2011.04.021.
[47] J.K. Saini, A.K. Patel, M. Adsul, R.R. Singhania, Cellulase adsorption on lignin : A roadblock for economic hydrolysis of biomass, Renew. Energy. 98 (2016) 29–42, https://doi.org/10.1016/j.renene.2016.03.089.
[48] M.M. Abu-Omar, K. Barta, G.T. Beckham, J.S. Luterbacher, J. Ralph, R. Rinaldi, Y. Román-Leshkov, J.S.M. Samec, B.F. Sels, F. Wang, Guidelines for performing lignin-first biorefining, Energy Environ. Sci. 14 (1) (2021) 262–292.
[49] W. Wang, L. Li, S. Tan, K. Wu, G. Zhu, Y. Liu, Y. Xu, Y. Yang, Preparation of NiS2// MoS2 catalysts by two-step hydrothermal method and their enhanced activity for hydrodeoxygenation of p-cresol, Fuel. 179 (2016) 1–9, https://doi.org/10.1016/j.fuel.2016.03.068.
[50] J.-Y. Kim, H.W. Lee, S.M. Lee, J. Jae, Y.-K. Park, Overview of the recent advances in lignocellulose liquefaction for producing biofuels, bio-based materials and chemicals, Bioresour. Technol. 279 (2019) 373–384, https://doi.org/10.1016/j.biortech.2019.01.055.
[51] S. Guadix-Montero, M. Sankar, Review on Catalytic Cleavage of C-C Inter-unit Linkages in Lignin Model Compounds: Towards Lignin Depolymerisation, Top. Catal. 61 (3-4) (2018) 183–198.
[52] J. Pu, T.S. Nguyen, E. Leclerc, C. Lorentz, D. Laurenti, I. Pitault, M. Tayakout-Fayolle, C. Geantet, Lignin catalytic hydroconversion in a semi-continuous reactor: An experimental study, Appl. Catal. B Environ. 256 (2019), 117769, https://doi.org/10.1016/j.apcatb.2019.117769.
[53] Z. Zhang, Q. Yang, H. Chen, K. Chen, X. Lu, P. Ouyang, J. Fu, J.G. Chen, In situ hydrogenation and decarboxylation of oleic acid into heptadecane over a Cu-Ni alloy catalyst using methanol as a hydrogen carrier, Green Chem. 20 (1) (2018) 197–205.
[54] I.G. Osojnik Črnivec, P. Djinović, B. Erjavec, A. Pintar, Low-temperature catalytic decarboxylation of formic and acetic acid over a Ru/TiO2 catalyst: prospects for continuous production of energy-rich gaseous mixtures, RSC Adv. 5 (2015) 54085–54089, https://doi.org/10.1039/C5RA08763E.
[55] E.D. N, Kinetic modeling of catalytic lignin hydroconversion for aromatic production These doctoral de L'Universite de Lyon. (2020).
[56] R.K. Chowdari, S. Agarwal, H.J. Heeres, Hydrotreatment of Kraft Lignin to Alkylphenolics and Aromatics Using Ni, Mo, and W Phosphides Supported on Activated Carbon, ACS Sustain. Chem. Eng. 7 (2019) 2044–2055, https://doi.org/10.1021/acssuschemeng.8b04411.
[57] L.F. Ramírez-Verduzco, M.J. Hernández-Sánchez, Blends of Green Diesel (Synthetized from Palm Oil) and Petroleum Diesel: a Study on the Density and Viscosity, BioEnergy Res. 14 (3) (2021) 1002–1013.
[58] H.Q. Lê, A. Zaitseva, J.-P. Pokki, M. Ståhl, V. Alopaeus, H. Sixta, Solubility of Organosolv Lignin in γ-Valerolactone/Water Binary Mixtures, ChemSusChem. 9 (2016) 2939–2947, https://doi.org/10.1002/cssc.201600655.
[59] G. Haarlemmer, C. Guizani, S. Anouti, M. Déniel, A. Roubaud, S. Valin, Analysis and comparison of bio-oils obtained by hydrothermal liquefaction and fast pyrolysis of beech wood, Fuel. 174 (2016) 180–188, https://doi.org/10.1016/j.fuel.2016.01.082.
[60] B. Joffres, M.T. Nguyen, D. Laurenti, C. Lorentz, V. Souchon, N. Charon, A. Daudin, A. Quignard, C. Geantet, Lignin hydroconversion on MoS2-based supported catalyst: Comprehensive analysis of products and reaction scheme, Appl. Catal. B Environ. 184 (2016) 153–162, https://doi.org/10.1016/j.apcatb.2015.11.005.
[61] B. Joffres, C. Lorentz, M. Vidalie, D. Laurenti, A.A. Quoineaud, N. Charon, A. Daudin, A. Quignard, C. Geantet, Catalytic hydroconversion of a wheat straw soda lignin: Characterization of the products and the lignin residue, Appl. Catal. B Environ. 145 (2014) 167–176, https://doi.org/10.1016/j.apcatb.2013.01.039.
[62] K.H. Kim, C.S. Kim, Recent Efforts to Prevent Undesirable Reactions From Fractionation to Depolymerization of Lignin: Toward Maximizing the Value From Lignin, Front. Energy Res. 6 (2018) 92. https://www.frontiersin.org/article/10.3389/fenrg.2018.00092.
[63] E. Bartolomei, Y. Le Brech, A. Dufour, V. Carre, F. Aubriet, E. Terrell, M. Garcia-Perez, P. Arnoux, Lignin Depolymerization: A Comparison of Methods to Analyze Monomers and Oligomers, ChemSusChem. 13 (2020) 4633–4648, https://doi.org/10.1002/cssc.202001126.
[64] M.I. Chudakov, Promyshlennoe ispol'zovanie lignina, Industrial Use of Lignin), Moscow Lesn. Promyshlennost'., 1983.
[65] D.S. Kosyakov, E.V. Ipatova, S.M. Krutov, N.V. Ul'yanovskii, I.I. Pikovskoi, Study of Products of the Alkaline Decomposition of Hydrolysis Lignin by Atmospheric Pressure Photoionization High-Resolution Mass Spectrometry, J. Anal. Chem. 72 (14) (2017) 1396–1403.
[66] C. Xu, R.A.D. Arancon, J. Labidi, R. Luque, Lignin depolymerisation strategies: towards valuable chemicals and fuels, Chem. Soc. Rev. 43 (2014) 7485–7500, https://doi.org/10.1039/C4CS00235K.
[67] M.M. Abu-Omar, K. Barta, G.T. Beckham, J.S. Luterbacher, J. Ralph, R. Rinaldi, Y. Román-Leshkov, J.S.M. Samec, B.F. Sels, F. Wang, Guidelines for performing lignin-first biorefining, Energy Environ. Sci. 14 (2021) 262–292, https://doi.org/10.1039/d0ee02870c.
[68] X. Huang, T.I. Korányi, M.D. Boot, E.J.M. Hensen, Ethanol as capping agent and formaldehyde scavenger for efficient depolymerization of lignin to aromatics, Green Chem. 17 (2015) 4941–4950, https://doi.org/10.1039/c5gc01120e.
[69] L. Shuai, B. Saha, Towards high-yield lignin monomer production, Green Chem. 19 (2017) 3752–3758, https://doi.org/10.1039/c7gc01676j.